Lung Cancer 182 (2023) 107283

Contents lists available at ScienceDirect

Lung Cancer

journal homepage: www.elsevier.com/locate/lungcan

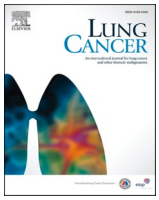

NSCLC presents metabolic heterogeneity, and there is still some leeway for EGF stimuli in *EGFR*-mutated NSCLC

Cindy Mendes [a,b], Isabel Lemos [a,b], Inês Francisco [b], Teresa Almodôvar [b], Fernando Cunha [b], Cristina Albuquerque [b], Luís G. Gonçalves [c], Jacinta Serpa [a,b,*]

[a] NOVA Medical School|Faculdade de Ciências Médicas, Universidade NOVA de Lisboa, Campo dos Mártires da Pátria, 130, 1169-056 Lisboa, Portugal
[b] Instituto Português de Oncologia de Lisboa Francisco Gentil (IPOLFG), Rua Prof Lima Basto, 1099-023 Lisboa, Portugal
[c] Instituto de Tecnologia Química e Biológica António Xavier (ITQB Nova), Oeiras, Portugal

ARTICLE INFO

Keywords:
Cancer metabolism
NSCLC
Metabolic heterogeneity
Metabolic-directed therapy

ABSTRACT

Background: Metabolic remodeling is crucial in carcinogenesis and cancer progression. Oncogenic mutations may promote metabolic reprogramming in cancer cells to support their energy and biomass requirements. EGFR mutations are commonly found in non-small cell lung cancer (NSCLC) and may induce NSCLC metabolic rewiring. Whether EGFR-driven metabolic reprogramming triggers cell vulnerabilities with therapeutic potential remains unknown.

Methods: The role of EGFR signaling activation by EGF was investigated using NSCLC cell lines with different *EGFR* and *KRAS* status: A549 (*EGFR* WT and *KRAS* c.34G > A), H292 (*EGFR* WT and *KRAS* WT) and PC-9 (*EGFR* exon 19 E746-A750 deletion and *KRAS* WT). The effect of EGF on NSCLC cell death and cell cycle was evaluated using flow cytometry, and cell migration was assessed through wound healing. EGFR, HER2, MCT1, and MCT4 expression was analyzed through immunofluorescence or western blotting. We explored the impact of glucose and lactate bioavailability on NSCLC cells' metabolic profile using nuclear magnetic resonance (NMR) spectroscopy. Moreover, the expression of several relevant metabolic genes in NSCLC cells or patient samples was determined by RT-qPCR.

Results: We showed that cell lines presented different metabolic profiles, and PC-9 cells were the most responsive to EGF stimulus, as they showed higher rates of cell proliferation and migration, together with altered metabolic behavior. By inhibiting EGFR with gefitinib, a decrease in glucose consumption was observed, which may be related to the fact that despite PC-9 harbor EGFR mutation, they still express the EGFR WT allele. The analysis of NSCLC patients' RNA showed a correlation between MCT1/MCT4 and GLUT1 expression in most cases, indicating that the metabolic information can serve as a reference in patients' follow-up.

Conclusion: Together, this study shows that NSCLC cell lines have heterogeneous metabolic profiles, which may be underlaid by different genetic profiles, revealing an opportunity to identify and stratify patients who can benefit from metabolism-targeted therapies.

1. Introduction

Lung cancer is a complex and heterogeneous disease, being the leading cause of cancer-related death worldwide, according to WHO, lung cancer is responsible for 1.59 million deaths globally per year [1]. This high mortality is a result of different factors: the late diagnosis – due to lack of symptoms in early stages; the molecular heterogeneity (consistent with difficulties in finding a specific treatment approach); and the chemotherapy and targeted therapy resistance phenomena [2,3]. Hence, the identification of suitable targets and markers to develop novel therapies and stratify patients is crucial.

Metabolic remodeling is one of the emerging hallmarks of cancer and due to the recognition of its vital role in cancer progression, it has gained more attention worldwide [4]. Cancer cells must reprogram their cellular metabolism to meet the high bioenergetic, biosynthetic, and redox demands of exponential cell proliferation and tumor growth [5,6].

* Corresponding author at: NOVA Medical School|Faculdade de Ciências Médicas, Universidade NOVA de Lisboa, Campo dos Mártires da Pátria, 130, 1169-056 Lisboa, Portugal.
E-mail address: jacinta.serpa@nms.unl.pt (J. Serpa).

https://doi.org/10.1016/j.lungcan.2023.107283
Received 20 April 2023; Received in revised form 15 June 2023; Accepted 19 June 2023
Available online 22 June 2023

Although metabolic patterns vary between malignant cells, glycolysis, glutamine catabolism, one-carbon metabolism, and redox homeostasis are generally altered [6–8]. These pathways are controlled intrinsically by oncogenic signaling and transcriptional networks but also extrinsically by tumor microenvironment factors (e. g. oxygen and nutrient availability, growth factors, cell-to-cell interactions) [7,9].

In the particular case of non-small cell lung cancer (NSCLC), it was described that glucose oxidation via PDH (pyruvate dehydrogenase) and the tricarboxylic acid (TCA) cycle were enhanced in tumors relative to adjacent benign lung tissue [10]. Additionally, lactate is a major fuel source for the TCA cycle in some NSCLC tumors [11]. In this context, monocarboxylate transporters (MCTs), which mediate lactate transport bidirectionally, are essential and allow cancer cells to transiently export lactate and import it to be subsequently used as a fuel for oxidative metabolism and gluconeogenesis [8,11–15].

It is well acknowledged that alterations in *KRAS*, the most frequently mutated oncogene in NSCLC (with a frequency around 25–35% [16]), alter cellular glucose uptake, glycolytic flux, and glutamine usage [17,18]. Moreover, tyrosine kinase receptor (RTK)-dependent signaling pathways induce metabolic remodeling, including the epidermal growth factor receptor 1 (*EGFR*), which plays crucial roles in cell differentiation, proliferation, migration, and invasion [19–22]. *EGFR* mutations have been detected in approximately 15–30% of tumors from the NSCLC group [19]. These mutations constitutively activate the EGFR tyrosine kinase domain, inducing an aberrant activation of signaling cascades, which promote pro-survival and anti-apoptotic signals through downstream targets [23]. Some of those pathways, such as the phosphatidylinositol 3-kinase (PI3K) pathway, also regulate metabolic remodeling, enhancing fatty acid synthesis and glycolytic flux [24]. Among all the metabolic changes observed in tumors, whether malignant cells with a specific oncogenic activation will show a defined metabolic preference is still uncertain [25].

In an *in vitro* NSCLC model, mutant *EGFR* was found to enhance glycolysis and pentose phosphate pathway (PPP), which altered pyrimidine biosynthesis and redox metabolism [26], reinforcing that glucose is a key substrate sustaining biosynthesis [6]. Nevertheless, *in vivo* validation of these findings is still needed. A more recent study showed that EGFR activation branched glycolysis to the serine synthesis for nucleotide synthesis and redox homeostasis in both *in vitro* and *in vivo* models of NSCLC [25]. Targeted therapy, implying the development of EGFR tyrosine kinase inhibitors (TKIs) was a great improvement for *EGFR*-mutated NSCLC patients' treatment, however, the highly metastatic properties and drug resistance mechanisms are still a problem [27]. Therefore, knowing the metabolic profiles dependent on the genetic status of NSCLC can be an opportunity to improve prognosis and design alternative therapies to overcome resistance to targeted therapy. Moreover, the combination of EGFR TKIs with drugs that exploit the metabolic vulnerabilities of NSCLC may unravel more effective approaches.

Our study aimed to explore, in an *in vitro* model, the role of EGF and EGFR-dependent pathways in the metabolic remodeling of NSCLC. Using NSCLC cell lines with different mutational status, we showed that NSCLC cell lines have heterogeneous metabolic profiles, which may be associated with a particular genetic profile, potentially laying the foundation for patient stratification in metabolism-targeted therapies.

2. Materials and methods

2.1. Cell lines and culture conditions

Human adenocarcinoma cell line A549 (CCL-185™, ATCC) and mucoepidermoid carcinoma cell line H292 (CRL-1848™, ATCC) were obtained from American Type Culture Collection (ATCC, Manassas, VA, USA) and adenocarcinoma cell line PC-9 (90071810, ECACC) was obtained from European Collection of Authenticated Cell Cultures (ECACC, Porton Down, Salisbury, United Kingdom). The selected NSCLC cell lines present different mutational profiles for *EGFR* and *KRAS*: A549 cells (*EGFR* WT (wild type) and *KRAS* c.34G > A (p.Gly12Ser); H292 cells (*EGFR* WT and *KRAS* WT), and PC-9 cells (*EGFR* exon 19 deletion (Ex19Del; Glu746-Ala750 deletion) and *KRAS* WT). Cells were cultured in Dulbecco's Modified Eagle's Medium 1× (DMEM) (41965-039, Gibco, Life Technologies) supplemented with 10% fetal bovine serum (FBS; S 0615, Merck), 1% Antibiotic-Antimycotic (AA; P06-07300, PAN Biotech) and 50 μg/mL Gentamicin (15750-060, Gibco, Life Technologies). Cells were maintained at 37 °C in a humidified environment with 5% CO_2. Cells were cultured until an optical confluence of 75–100% and detachment was performed with 0.05% trypsin-EDTA 1× (25300-054, Invitrogen). Before any *in vitro* experiment, cells were synchronized under starvation (FBS-free culture medium) overnight. For experimental conditions, cells were cultured for 24 h, in 1% FBS-supplemented glucose-free DMEM (P04-01549, Pan-Biotech) supplemented with 0.58 g/L L-glutamine, with or without 10 mM sodium lactate (NaLac) and in 1% FBS supplemented DMEM with 4.5 g/L glucose. All conditions were tested with or without 0.025 μg/ml EGF (E9644, Sigma-Aldrich, MO, USA). In EGFR inhibition assays, cells were also exposed to gefitinib (20 μM, SML1657, Sigma-Aldrich, MO, USA) for 24 h. The gefitinib concentration was chosen in accordance with the half-maximal effective concentration determined in NSCLC cells (EC50; see Supplementary Fig. 1).

2.2. Cell cycle assay

Cell cycle status was determined by flow cytometry, cells were seed in 12-well plates (2×10^5 cells /well), exposed to experimental conditions, and afterward collected, fixed in 70% ethanol (100983, Merck) and stored at 4°C, for 6 h (minimum). Cells were centrifuged at 155 × *g* for 5 min at 4 °C, suspended in 100 μL of propidium iodide (PI) solution (50 μg/mL PI, 0.1 mg/mL RnaseA (RN-001, Citogene) and 0.05% Triton X-100) and incubated for 40 min at 37 °C. Cells were centrifuged at 155 × *g* for 10 min at 4 °C, the supernatant was discarded, and cells were resuspended in 200 μL 1 × PBS + 0.1% (v/w) BSA. Samples were analyzed by flow cytometry (FACScalibur – Becton Dickinson), using FlowJo 8.7 software (https://www.flowjo.com). Experiments were performed in biological triplicates.

2.3. Proliferation curves

Cell proliferation analysis was determined by the establishment of proliferation curves, cells were seeded in 24-well plates (5×10^4 cells/well) in complete DMEM, synchronized under starvation, and exposed to the experimental conditions. Cells in suspension in the culture medium and adherent/trypsinized cells were counted at different time points (0, 6, 10, 24, 32, and 48 h) using a Bürker cell counting chamber.

2.4. Calculation of cell population doubling time

Population doubling time (DT) or the time required for a culture to double the number of cells was calculated according to ATCC® Animal cell culture Guide, using the following formula:

$$DT = \frac{Tln(2)}{\ln(\frac{Xe}{Xb})}$$

In which T is the incubation time in any units, Xb is the cell number at the beginning of the incubation time and Xe is the cell number at the end of the incubation time.

2.5. Wound healing assay

The migratory capacity of cells was examined by the wound healing assay. Cells were seeded in 12-well plates (2×10^5 cells /well) in complete DMEM and maintained until 70–80% confluence. The cells

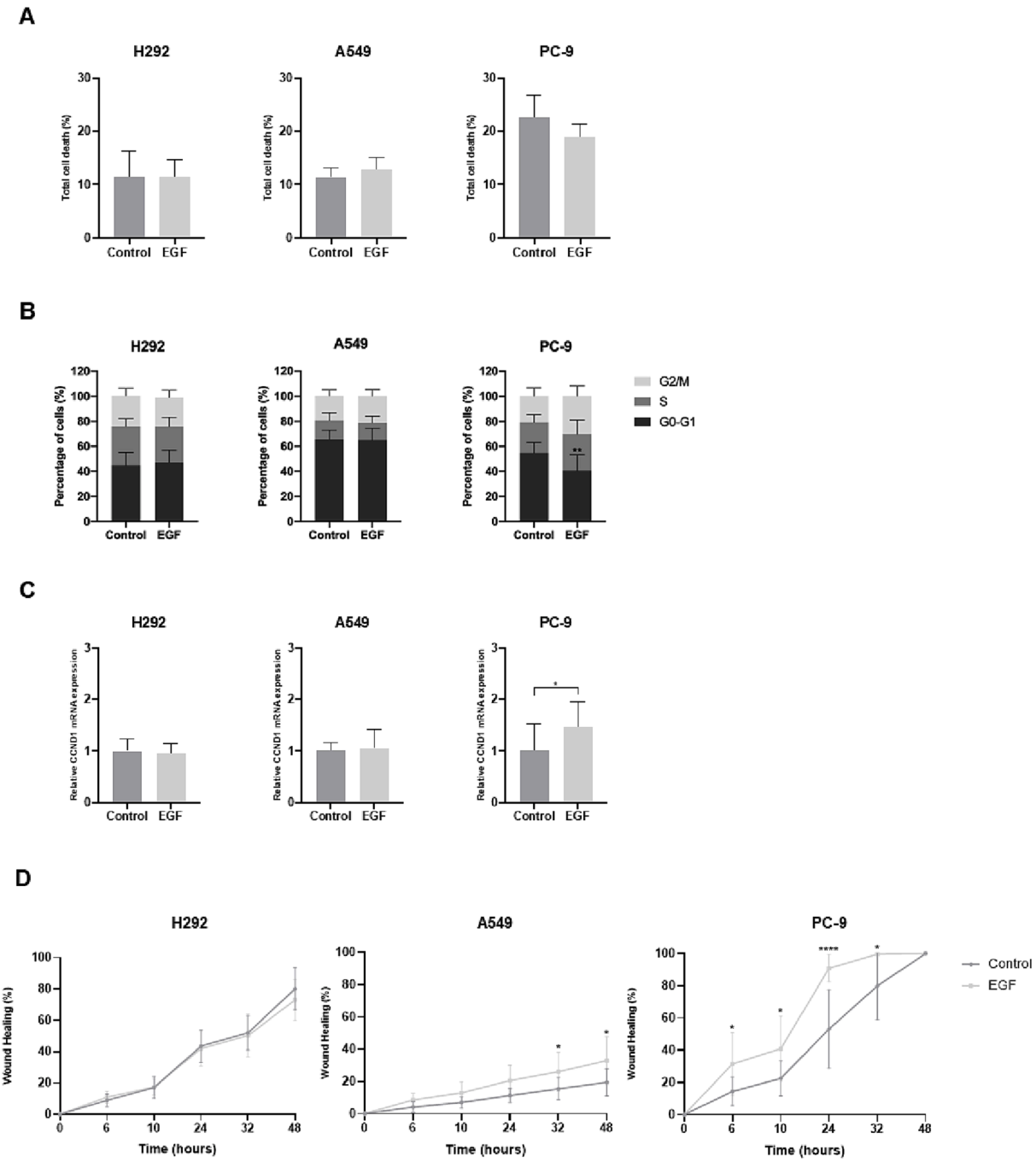

Fig. 1. EGFR mutated cell line PC-9 (EGFR$^{delE746-A750}$ ∧ KRAS^{WT}) is the most responsive to EGF stimulus. Cells were cultured in control and EGF conditions for 24 h. (A) Percentage of cell death analyzed by flow cytometry using Annexin V and PI. (B) Cell cycle analysis by flow cytometry in ethanol-fixed cells stained with propidium iodide (PI). (C) Relative gene expression of CCDN1. HPRT gene was used as endogenous control. Expression levels were normalized to those obtained for cells cultured in control conditions. (D) Quantification of wound closure in cells cultured in control and EGF conditions for 0, 6, 10, 24, 32, and 48 h. Results are shown as mean ± SD. *p < 0.05, **p < 0.01, ***p < 0.001. Unpaired *t*-test and two-way ANOVA with Tukey's test were used.

were previously treated with Mitomycin-C (5 μg/mL, M4287, Sigma), and after 3 h the cell monolayer was scratched with a 200 μL pipette tip to create a wound. Cells were washed in PBS 1 × and maintained in experimental conditions. Wound closure was monitored by photography at 0, 6, 10, 24, 32, and 48 h using phase-contrast microscopy with the Olympus IX53 Inverted Microscope. Images were acquired and processed with Olympus cellSens software. ImageJ software (https://imagej.nih.gov) was used to analyze and quantify the images.

2.6. Cell death analysis

Cell death analysis was assessed by flow cytometry. After experimental conditions, supernatants (conditioned culture media) were collected, and cells were harvested with trypsin and centrifuged, together with cells in the supernatant, at 150 × *g* for 2 min. Cells were suspended with 0.5 μL Annexin V- fluorescein (FITC)- (640906, BioLegend) in annexin V binding buffer 1 × and incubated at RT, in the dark for 15 min. After incubation, samples were resuspended in 200 μL PBS 1 × − 0.1% (v/w) BSA and centrifuged at 155 × *g* for 2 min. Cells were

resuspended in 100 μL of annexin V binding buffer 1 × and 2.5 μL propidium iodide (PI, 50 μg/mL; P4170, Sigma-Aldrich) was added and samples were analyzed by flow cytometry (FACScalibur – Becton Dickinson), using FlowJo 8.7 software (https://www.flowjo.com). Experiments were performed in biological triplicates.

2.7. Nuclear magnetic resonance (NMR) spectroscopy

Nuclear Magnetic Resonance (NMR) spectroscopy was performed for all cell lines. Cells were plated in 175 cm^2 T-Flasks: H292 (1.5×10^7 cells/flask); A549 (2×10^7 cells/flask), and PC-9 (2.5×10^7 cells/flask). Cells were exposed to 5 mM D-glucose or 10 mM sodium lactate (NaLac); with or without 0.025 μg/mL EGF in glucose-free DMEM (P04-01549, Pan-Biotech), supplemented with 0.58 g/L L-glutamine, 1% FBS, 1% AA, for 24 h. Culture media was collected and stored at − 80 °C.

Cell methanol/chloroform/water extracts were performed to separate the aqueous (methanol/water) and organic (chloroform) phases. The aqueous phase was lyophilized in a SpeedVac Plus system and was suspended in deuterated water (D_2O) with 0.04% (v/v) azide, and 0.22 mM 3-(trimethylsilyl)propionic2,2,3,3-d4 acid (TSP) was used as chemical shift reference and concentration standard. For extracellular metabolites analysis, 30 μL of 2.2 mM TSP and 30 μL of 0.4% (v/v) sodium azide in D_2O were added to 540 μL of supernatants. ^1H NMR spectra were obtained at 25 °C in an UltrashieldTM Avance 500 Plus spectrometer (Bruker) equipped with a TCI-Z probe. Spectra were acquired and processed using TopSpin 4.1 software (Bruker) and the assignments were made by resorting to spectral databases: Human Metabolome (HMDB) and Chenomx NMR Suite 8.11 were used to determine the concentration of the metabolites.

2.8. Quantitative real-time PCR (qPCR)

Total RNA was extracted using RNeasy Mini Extraction kit (74,104, Qiagen, Hilden, Germany) and cDNA synthesized from 1 μg RNA by SuperScript II Reverse Transcriptase (18080e44, Invitrogen), both according to the manufacturer's protocol.

RNA was extracted from formalin-fixed paraffin-embedded (FFPE) NSCLC samples collected in *Instituto Português de Oncologia de Lisboa Francisco Gentil*, EPE (IPOLFG, EPE), using semi-automatic isolation with the Maxwell purification system (Maxwell RSC RNA FFPE Kit, AS1440, Promega) and cDNA was synthesized as mentioned above. Quantitative Real-Time PCR (qPCR) was performed using SYBR Green PCR Master Mix (04707516001, Roche), according to the manufacturer's protocol and the specific primers and genes are presented in Table 1.

Real-time PCR was carried out during 40 amplification cycles, according to the manufacturer's instructions, using a Lightcycler® 480 System instrument (05015243001, Roche). *Hypoxanthine-guanine phosphoribosyltransferase* (*HPRT*) was used as a housekeeping gene (Table 1). Experiments were performed in biological triplicates.

2.9. Next-generation sequencing for mutation detection

Somatic mutational data for *EGFR*, *KRAS*, *BRAF*, *ALK*, *ROS1,* and *MET* genes was obtained from 55 NSCLC samples in the context of the mutation analysis performed for clinical management according to standard guidelines (IPOLFG Ethical Committee Ref: UIC/1442). Briefly, the analysis was performed by Next-Generation Sequencing (NGS), using the Ampliseq™ Focus Panel kit (Illumina), on the Miseq platform (Illumina), with a minimum depth coverage of 500x. Bioinformatics analysis was performed using DNA + RNA Amplicon v.1.0.5 software (Illumina) for alignment and Alissa Interpret v.5.3.4 (Agilent Technologies) for analysis and annotation of the genetic variants.

2.10. Immunofluorescence

Immunofluorescence was used to detect the expression of certain proteins. Cells (1×10^5 cells/well) were seeded on glass slides with a 0.2% gelatin coating, until 80% of confluence and then fixed in 2% paraformaldehyde for 15 min at 4ºC. After fixation, cells were incubated with 50 mM ammonium chloride (NH4Cl) for 10 min. Blocking and antibodies dilution were performed with PBS 1× − 0.5% BSA − 0.1% saponin-PBS (w/v/v), between incubations, cells were rinsed twice with PBS 1×, for 5 min. After blocking for 1 h, slides were incubated with rabbit anti-human MCT1 (1:500, ab179832, Abcam), mouse anti-human MCT4 (1:100, SC-376140, Santa Cruz), rabbit anti-human EGFR (1:200, ab131498, Abcam) and rabbit anti-human HER2 (1:200, ab16901, Abcam) overnight at 4 °C. Cells were incubated with the Alexa Fluor 488 goat anti-rabbit (1:1000 in; A-11078, Invitrogen - Thermo Fisher Scientific) for 2 h at room temperature.

The slides were mounted in VECTASHIELD media with DAPI (4′-6-diamidino-2-phenylindole) (Vector Labs) and examined by standard fluorescence microscopy under a Zeiss Imager.Z1 AX10 microscope. Images were acquired and processed with CytoVision software and quantified with ImageJ software.

Table 1
Presentation of the target genes and designation and sequence (5′-3′) of primers used in RT-qPCR.

Reference/Target	Primers (5′-3′)
SLC16A1 (encoding MCT1)	For: GCTGGGCAGTGGTAATTGGARev: CAGTAATTGATTTGGGAAATGCAT
SLC16A3 (encoding MCT4)	For: CACAAGTTCTCCAGTGCCATTGRev: CGCATCCAGGAGTTTGCCTC3
GLUT1	For: CACGGCCTTCACTGTCGTGRev: GGACATCCAGGGTAGCTGC
SGLT1	For: CACAGGGTCTCTGGTCTGCRev: CATGATGAACATGGGCATCAG
LDHA	For: CTTGCTCTTGTTGATGTCATCGRev: CAGCCGTGATAATGACCAGC
LDHB	For: GAGCCTTCTCTCTCCTGTGRev: CTGATAGCACACGCCATACC
PEPCK/PCK1	For: GCGGATCATGACGCGGATGRev: GAGCGTCAGCTCCGGGTTG
PCK2	For: CAAGACCAACCTGGCTATGATGRev: GAGTCGACCTTCACTGTCAAAC
PFKFB1	For: CCAGTATCGACGAGAGGCAGRev: CTCTGGTAGTGTTGGTGGCATC
ALT	For: CGTGACGGTGCTGAAGCTGRev: CTCGTCCAGGTAGTAATCCAC
G6PD	For: GGCAACAGATACAAGAACGTGAAGRev: GCAGAAGACGTCCAGGATGAG
EGFR WT	For: GTTCGCACGGTGTATAAGGRev: CACGCTGGCCATCACGTAG
EGFR exon 19 deletion	For: CCGTCGCTATCAAGACATCTCRev: CACGCTGGCCATCACGTAG
HPRT	For: TGACACTGGCAAAACAATGCARev: GGTCGTTTTTCACCAGCAAGCT

2.11. Western blotting

Total protein extracts were obtained after cell lysis in 20 mM MOPS (pH 6.5), 1% Triton X100 (v/w) previously supplemented with 1 mM Na_3VO_4, 1 mM NaF, and 1X protease inhibitors (11836170001, Roche). Protein concentration was established by the Bradford method, using Bio-Rad protein assay reagent (500–0006, Bio-Rad) through spectrophotometric quantification (595 nm). After protein quantification, loading buffer containing 10% SDS, 0.5% bromophenol blue in Tris-HCL (pH 6.8), and 10% β-mercaptoethanol (M3148, Sigma) was added to each cell lysate and boiled at 95–100 °C for 10 min. Total protein (100 μg) was loaded in 12% polyacrylamide gel (Tris-glycine SDS-Polyacrylamide gel) and electrophoresis was carried out in MINI-PROTEAN Tetra Electrophoresis System (Bio-Rad). After, proteins were transferred to nitrocellulose membranes (Bio-rad) with the Trans-Blot® Turbo TM Blotting system. For protein detection, membranes were incubated with the primary specific antibodies anti-EGFR (1:1000;

ab131498, Abcam), anti-MCT1 (1:500; ab179832, Abcam) anti-phospho-AKT (1:1000, 9271, Cell Signalling), anti-phospho-ERK1/2 (1:1000, 9101, Cell Signalling) and anti-phospho-Src (1:1000, 2101, Cell Signalling) at 4 °C overnight. Blots were further incubated with anti-rabbit horseradish peroxidase (HRP)-conjugated secondary antibody (1:5000, 31460, Thermo Scientific) for 2 h at room temperature, and immunoreactive bands were detected using the enhanced chemiluminescence (ECL) method in a ChemiDoc XRS System (Bio-Rad) with Image Lab software. As endogenous control β-actin was used, membranes were re-incubated using mouse anti-human β actin (1:5000, A5441, Sigma). Experiments were performed in biological triplicates.

2.12. WST-1 assay for cell metabolic viability

The WST-1-based colorimetric assay (Roche Applied Science, Indianapolis, IN, USA) was performed to quantify cell metabolic viability. Cells were seeded in 96-well clear bottom tissue culture plates and treated at different concentrations and time points. Cells were incubated with WST-1 reagent for 1 h at 37 °C with 5% CO_2. In actively metabolizing cells, the WST-1 reagent is cleaved to formazan by cellular enzymes. The presence of formazan was assessed through spectrophotometric quantification (450 nm) in Bio-Rad iMark (1681130) microplate reader.

2.13. Luciferase reporter gene assay

To evaluate the activity of MCT1 promoters after EGF stimulation of NSCLC cells cultured in the presence and absence of lactate and glucose, two different MCT1 promoter pGL3basic (Firefly luciferase) deletion constructs (mct1 f1 and mct1 f2) were generated using respectively with primers Forward 1 (*Mlu* I restriction): ATGACGCGTGATTGCCTAGAGCTCGTCAG and Forward 2 (*Mlu* I restriction): ATGACGCGTGGACATCAAAGACACTCCATG paired with primers Reverse (*Hind* III restriction): ATGAAGCTTCTGCCTCGTTTGCTTGTTCC and conventional molecular cloning techniques, as described in [28,29]. After co-transfection, both Firefly and Renilla luciferase activities were measured sequentially in cell lysates, using a Dual-Luciferase reporter system (E1910; Promega) in a VICTOR™ X Light Luminescence Plate Reader (PerkinElmer).

2.14. Statistical analysis

Statistical analysis was performed using GraphPad Prism 6.0 software (https://www.graphpad.com). Sample data were presented as the mean (normal distribution) ± SD. Assays were performed with at least three biological replicates per treatment. Comparisons between data from each group were statistically analyzed by a two-tailed unpaired Student's *t*-test and multiple comparisons were performed using One-way ANOVA with Dunnett's or Tukey's test. For comparisons of two groups, a two-tailed independent-samples *t*-test was used. For cell cycle and proliferation curves analysis, a Two-way ANOVA with Tukey's test was used. To assess differences in gene expression levels in samples from NSCLC tumors, 2-sided independent samples Kruskal-Wallis One-way ANOVA with multiple comparisons or Mann-Whitney test was performed, where the adjusted significance was considered. In this context, the existence of a linear relationship between two variables was investigated using a two-tailed Spearman correlation test. Differences between experimental conditions were considered statistically significant at $p < 0.05$. Multivariate statistical analysis of ^{1}H NMR data was performed on MetaboAnalyst 5.0 (assessed on 16 November 2022) using metabolites concentrations as inputs and scaled using pareto-scaling. Heatmaps representing the univariate analysis of the intracellular and extracellular levels of the different metabolites detected by NMR were created for each cell line using GraphPad Prism 6.0 software.

3. Results

3.1. EGFR mutated cell line PC-9 ($EGFR^{delE746\text{-}A750} \wedge KRAS^{WT}$) is the most responsive to EGF stimuli

The effect of EGF on different phenotypic characteristics of NSCLC was assessed in control conditions and under EGF stimulus during 24 h (Fig. 1). Considering cell death, no statistical differences were observed between control cells and cells exposed to EGF, but in PC-9 cells, EGF induced a trend to decrease cell death (Fig. 1 A). While no significant differences were found in terms of the cell cycle in A549 and H292, in PC-9 cells exposed to EGF, the G0-G1 phase was significantly decreased, with a corresponding increase in the percentage of cells dividing (S + G2/M phases) (Fig. 1 B). In agreement, the relative expression of *CCDN1* (encoding Cyclin D1) was significantly augmented with EGF exposure in PC-9 cells (Fig. 1 C). *CCDN1* expression is regulated by AP1 involved in EGFR-dependent pathways.

Regarding cell migration PC-9 exhibited a higher migratory potential, closing the wound within 48 h, which was not observed in A549 and H292 (Fig. 1 D). EGF promoted significant differences in the percentage of wound closure in PC-9 cells at every time point, while in A549 it only had an effect at later timepoints (32 and 48 h).

The expression of the EGF receptors, EGFR and HER2, was also evaluated to better understand the changes observed in the EGF-stimulating capacity and to verify if EGF was able to regulate the expression of its receptors. We analyzed EGFR protein expression through immunofluorescence and western blotting. EGF induced a significant decrease in EGFR expression in A549 cells while the opposite was observed in PC-9 cells (Fig. 2 A and B). By western blotting, EGF increased the expression of EGFR in H292 and PC-9 cells (Fig. 2 C). We also analyzed the expression of WT and delE746-A750 variants of *EGFR* mRNA in PC-9 cells by qRT-PCR. This cell line mostly expresses the mutated variant of *EGFR* (80%) but the WT variant is still expressed (20%) (Fig. 2 D), and this ratio is maintained upon EGF exposure. Regarding HER2 expression, once again, PC-9 cells showed an increased expression after EGF exposure (Fig. 2 E and F). On the other hand, EGF significantly reduced HER2 in H292.

3.2. EGF significantly regulates the levels of MCT1 and MCT4 in PC-9 ($EGFR^{delE746\text{-}A750} \wedge KRAS^{WT}$)

Subsequently, we assessed EGF interference in the regulation of the expression of genes essential for the modulation and maintenance of glucose and lactate metabolism. We evaluated the levels of MCT1 and MCT4 by immunofluorescence and western blot. We found that H292 and PC-9 cells treated with EGF presented significantly augmented MCT1 expression (Fig. 3 A and B). Looking at the basal levels of MCT1, H292 were the cells that expressed this protein the most, and A549 cells were the ones expressing the lowest levels (Fig. 3 C and D). By NMR, the basal intracellular levels of lactate were measured, and H292 cells accumulated lower levels of lactate, followed by PC-9 and A549 (Fig. 3 E). As regards MCT4, no meaningful changes were observed in H292 and A549 due to EGF exposure, while PC-9 EGF-treated cells showed increased MCT4 expression (Fig. 3 F and G). Considering basal levels, H292 are the cells with the highest MCT4 expression, followed by PC-9 and A549 (Fig. 3 H). The levels of lactate in the extracellular media suggested that PC-9 cells exported more lactate than H292 and A549 (Fig. 3 I).

3.3. NSCLC cells exhibit distinct metabolic profiles

Afterward, we explored the impact of glucose and lactate bioavailability on NSCLC cells' metabolic profile. The impact of glucose and lactate in cellular metabolism was characterized for the three cell lines by NMR spectroscopy using the metabolites identified in both supernatants (extracellular) and methanolic cell extracts (intracellular). The

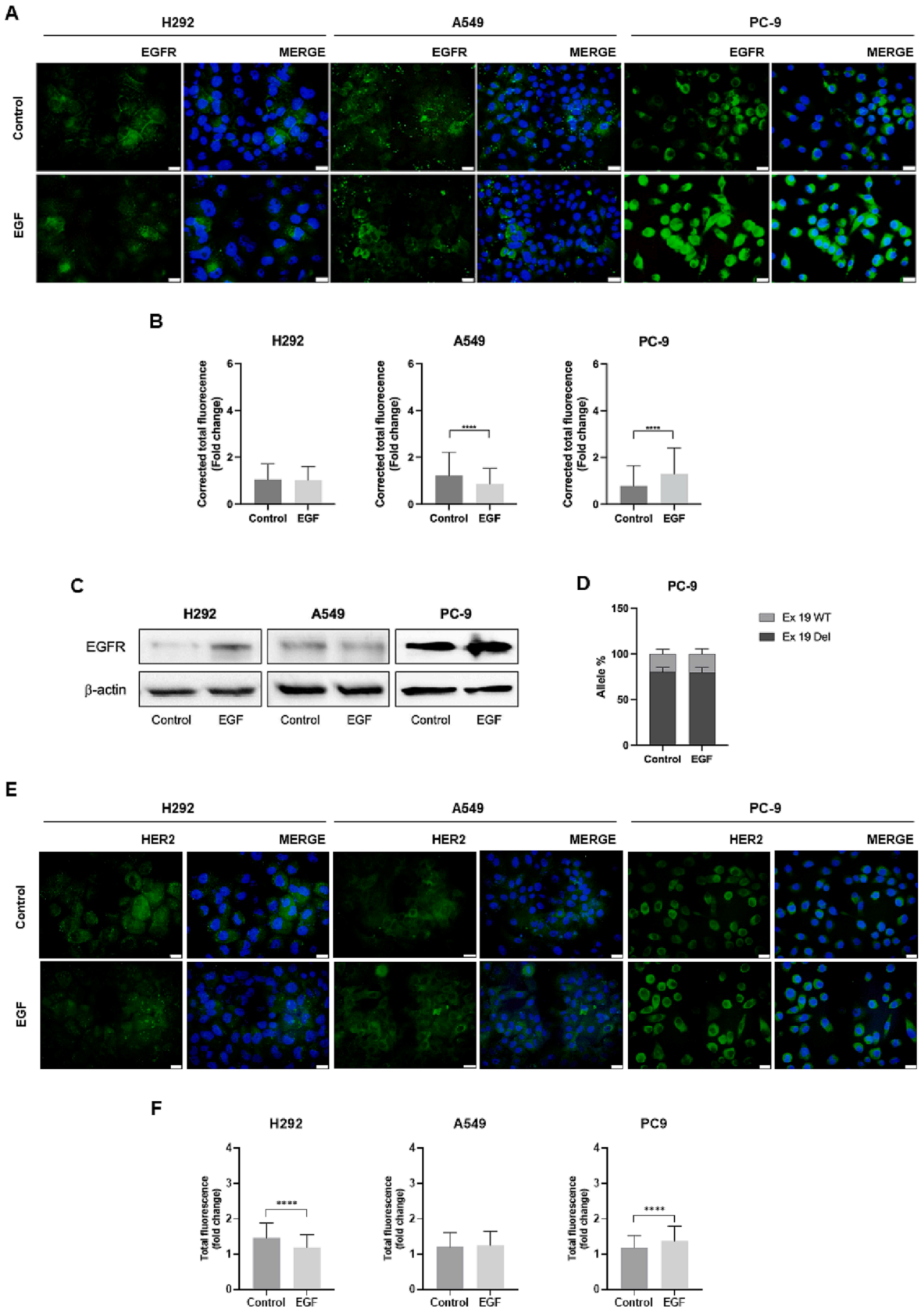

Fig. 2. EGF increases the expression of EGFR and HER2 in PC-9 cells. Cells were cultured in control and EGF conditions for 24 h. **(A)** EGFR expression by immunofluorescence and **(C)** by western blotting. **(B)** EGFR immunofluorescence quantification (CTCF) using the ImageJ program. **(D)** Relative expression of *EGFR* WT and exon 19 deletion mutated variants in PC-9 cells. **(E)** HER2 expression by immunofluorescence and **(F)** respective quantification (CTCF). Results are shown as mean ± SD *p < 0.05, **p < 0.01, ***p < 0.001. An unpaired *t*-test was used.

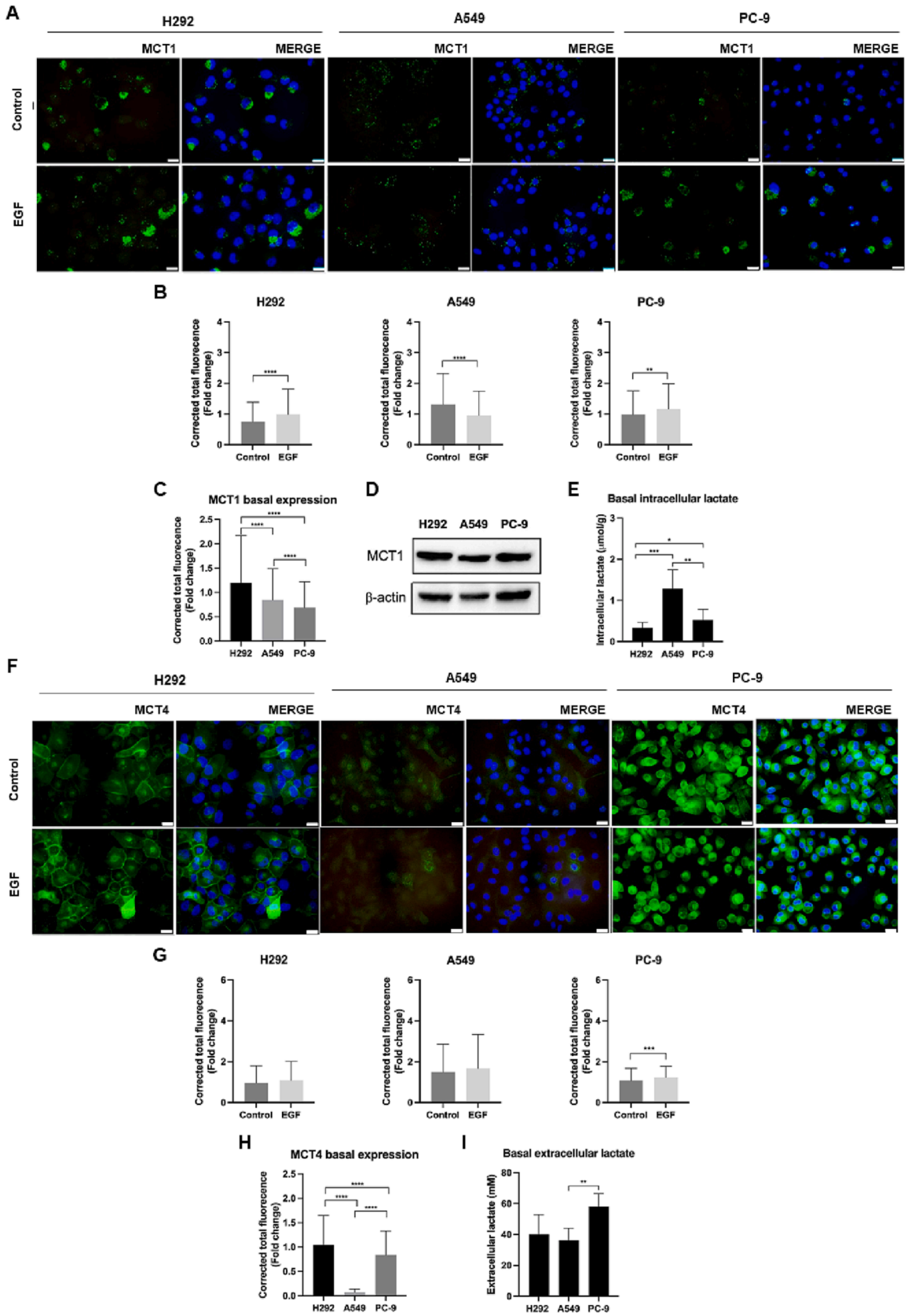

Fig. 3. EGF increases MCT1 expression in H292 and PC-9 cells and MCT4 expression in PC-9 cells, and cells expressing higher levels of MCT1 show lower levels of intracellular lactate. Cells were cultured in control and EGF conditions for 24 h. Immunofluorescence for the detection of **(A)** MCT1 and **(F)** MCT4, which were respectively quantified using ImageJ program **(B and G)**. Basal protein levels of MCT1 by immunofluorescence **(C)** and by western blotting **(D)**. Basal MCT4 protein levels by immunofluorescence **(H)**. Basal intracellular **(E)** and extracellular **(I)** levels of lactate. Results are shown as mean ± SD *p < 0.05, **p < 0.01, ***p < 0.001. Unpaired *t*-test or one-way ANOVA with Tukey's test were used.

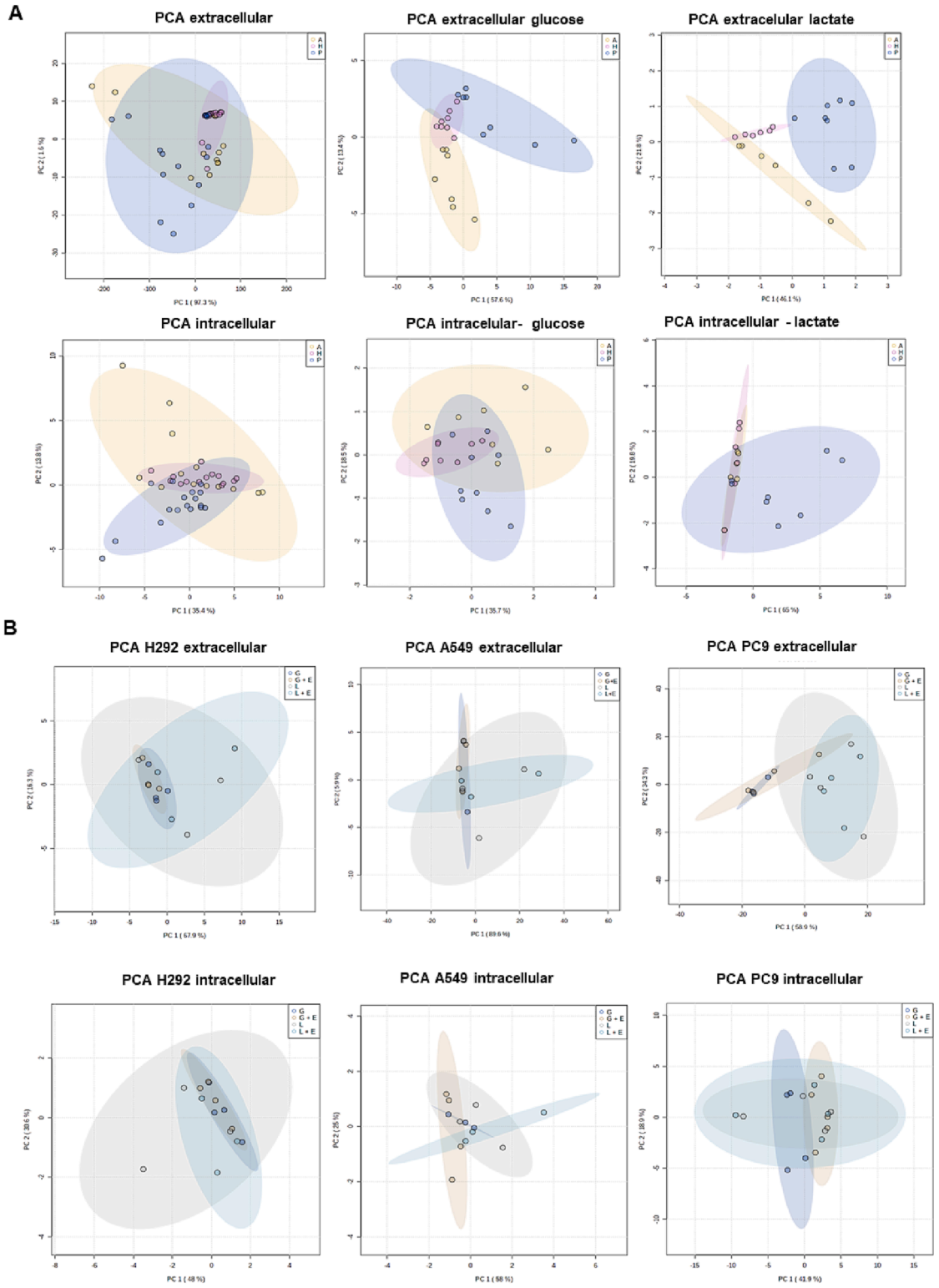

Fig. 4. Lung cancer cells show distinct metabolic profiles, lactate potentiates differences in the metabolic profile of each cell line while glucose only exerts an effect on PC-9 cells exposed to EGF, which is rescued by gefitinib. Cells were cultured in the presence of glucose or lactate, with or without EGF stimulation, and PC-9 cells were exposed to gefitinib. **(A)** Principal component analysis (PCA) score plots depict the clustering patterns from ^{1}H NMR metabolomic profiles among the three lung cancer cell lines. **(B)** PCA score plots of metabolome data for each lung cancer cell line from supernatant samples (top) and cell extracts (bottom). **(C, D, E)** Heatmap showing the levels of intracellular and extracellular metabolites in H292, A549, and PC-9 cells, respectively. **(F)** PCA score plots of metabolome data of PC-9 cells in the presence of glucose. **(G)** Heatmap of 35 identified metabolites on PC9 cell extracts in the presence of glucose. The color code inside the heatmap depicts the relative fold change of each metabolite between classes, red and blue colors express increased or decreased levels, respectively. The parameters that were used for the analysis were the Euclidean distance measure and the Ward cluster algorithm, using MetaboloAnalyst 5.0 software.

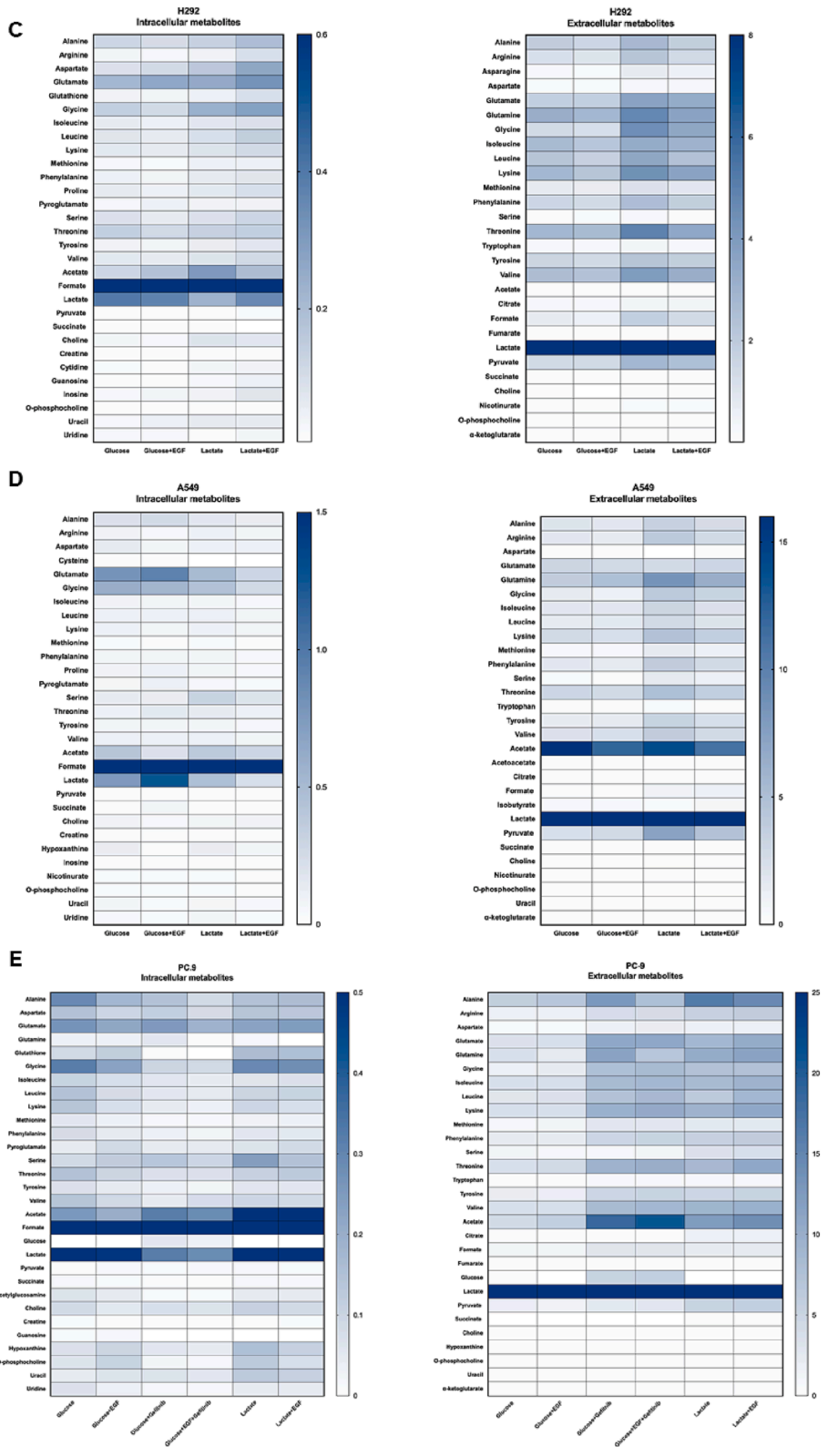

Fig. 4. (*continued*).

specific metabolic patterns were assessed using principal component analysis (PCA). The exometabolome of each cell line shows a different profile depending on the carbon source (Fig. 4 A). A clustering by cell line is observed on the PCA scores plots of metabolites from H292, A549, and PC-9 cells. The carbon source does not appear to influence the exometabolome of H292 cells since they form well-defined clusters in both conditions, while A549 and PC-9 seem to be more heterogeneous. Interestingly, lactate potentiates differences in the metabolic profile of each cell line. Additionally, the PCA scores of A549 and H292 intracellular metabolites in the presence of lactate overlap.

Heatmaps representing the univariate analysis of the intracellular and extracellular levels of the different metabolites detected by NMR

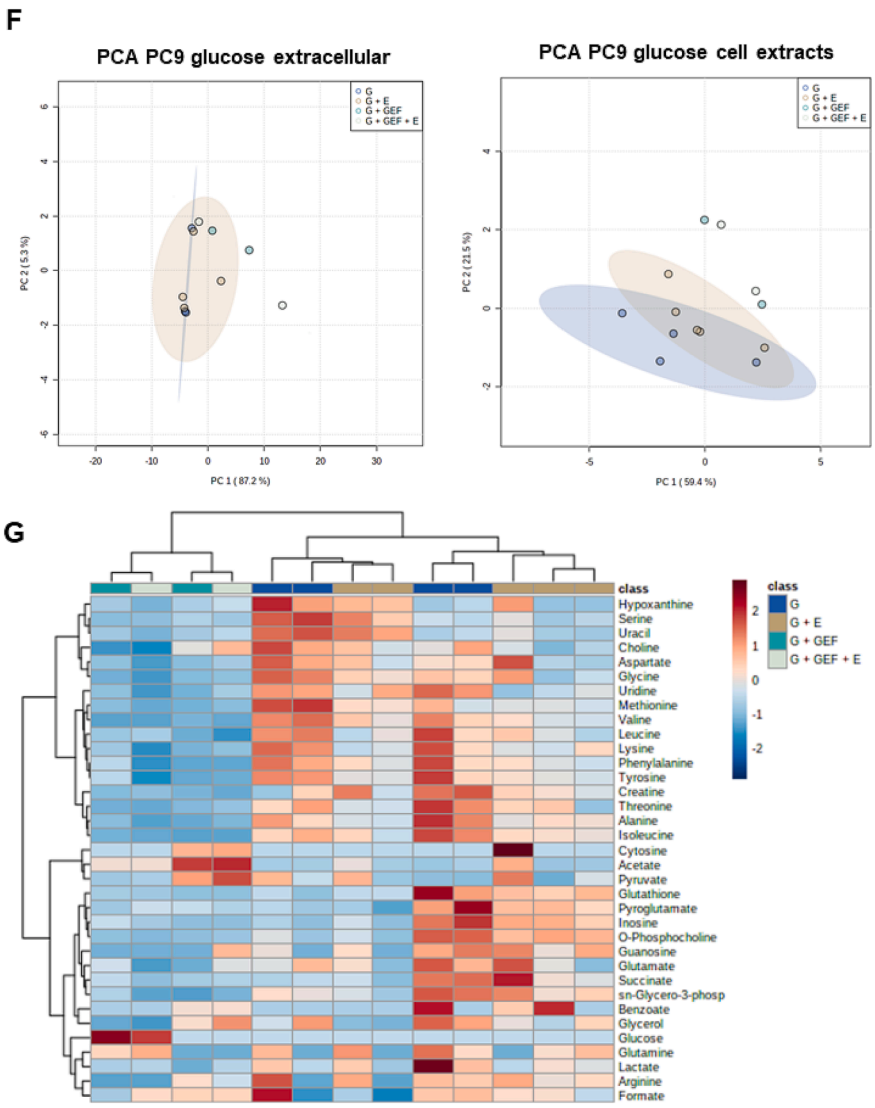

Fig. 4. (*continued*).

were created for each cell line (Fig. 4 C, D, E). The detailed concentrations obtained for each metabolite in H292, A549, and PC-9 are depicted respectively in Supplementary Figs. 2, 3, and 4.

3.4. Lactate in combination with EGF fuels the TCA cycle and increases the synthesis of nitrogenous bases in H292 cells

In H292 cells cultured with glucose, EGF had no significant effect both intra and extracellularly. H292 proved to be a cell line well adapted to lactate and under lactate plus EGF conditions, a tendency to increase the levels of most amino acids was observed, at the intracellular level (Fig. 4 C, Supplementary Fig. 2 A). In EGF-treated H292 cells, an increase in the levels of aspartate, glutamate, and glycine was observed upon lactate exposure (Fig. 4 C, Supplementary Fig. 2 A). Glutathione levels tended to increase in cells exposed to lactate plus EGF. Formate intracellular levels were also augmented in H292 upon lactate exposure (Fig. 4 C, Supplementary Fig. 2B), being this increase abolished by EGF. Lactate in combination with EGF tended to increase lactate and pyruvate intracellular levels (Fig. 4C, Supplementary Fig. 2B), and intracellular choline was increased by lactate independently of EGF (Fig. 4 C, Supplementary Fig. 2 C). H292 cells stimulated with EGF plus lactate revealed increased levels of guanosine, cytidine, and inosine, which are nitrogen bases needed for nucleotide synthesis (Fig. 4 C, Supplementary Fig. 2 C). Regarding the extracellular media, lactate increased the levels of glutamate, glutamine, glycine, lysine, and threonine, while glutamine was significantly reduced after lactate plus EGF exposure when compared to lactate alone (Fig. 4 C, Supplementary Fig. 2 D). Interestingly, asparagine (whose precursor is oxaloacetate) was detected in the media of H292 cells, which did not occur in the other cell lines. Moreover, EGF in combination with lactate decreased lactate levels, when comparing to lactate alone (Fig. 4 C, Supplementary Fig. 2 E). Additionally, citrate levels tended to be higher in lactate-treated cells. These findings indicate that lactate in combination with EGF fueled the TCA cycle and boosted nitrogen bases synthesis in H292 cells.

3.5. Glutamine catabolism is increased, and fatty acid oxidation is active in A549

A549 cells showed to be adapted to glucose and lactate consumption and the main statistical differences in each culture condition are further highlighted. EGF induced a significant increase in glutamate intracellular levels and a trend to augment alanine in glucose-treated cells (Fig. 4 D, Supplementary Fig. 3 A). Cysteine was only detected in A549 cells exposed to glucose, and neither glutathione nor glutamine were found in the intracellular extracts. Hypoxanthine intracellular levels decreased significantly after glucose plus EGF exposure (Fig. 4 D,

Supplementary Fig. 3 C). Moreover, lactate decreased the levels of glutamate and glycine, and EGF exacerbated this effect. Acetate tended to be higher in lactate conditions, while lactate tended to be lower (Fig. 4 D, Supplementary Fig. 3 B). Considering the extracellular media, the levels of arginine and phenylalanine were increased in A549 cells exposed to lactate plus EGF (Fig. 4 D, Supplementary Fig. 3 D). Lactate independently of EGF augmented the levels of glutamine and lactate (Fig. 4 D, Supplementary Fig. 3 D, and E). Non-significant differences were found in formate and choline levels, however, a trend to increase these compounds levels was observed under lactate conditions (Fig. 4 D, Supplementary Fig. 3 E, and F). Interestingly, two end products of fatty acid β-oxidation, acetoacetate, and isobutyrate, were only detected in A549 (Fig. 4 D, Supplementary Fig. 3 E), not in the other cell lines. These results suggest that in A549 cells glutamine catabolism is increased, and fatty acid oxidation is active.

3.6. EGF impacts PC-9 glucose metabolism and gefitinib promotes the loss of the EGF effect

In the multivariate analysis through PCA scores, the global effect of EGF on the metabolite profile of H292 and A549 cells does not allow the separation of the experimental conditions (Fig. 4 B). However, EGF induced an effect in PC-9 cells exposed to glucose as in intracellular extracts there is a clear formation of two clusters of cells incubated with glucose and cells incubated with glucose in the presence of EGF. In cells exposed to lactate, EGF has no influence. In addition, the exometabolome of PC-9 shows a separation by carbon source, which is motivated by increased levels of acetate, alanine, glutamate, and glutamine when lactate is the carbon source.

Regarding PC-9 metabolic profile responsive to EGF, we evaluated the effect of EGFR TKI gefitinib to confirm the influence of EGF on PC-9 cells' metabolic behavior, in cells cultured with glucose in the presence and absence of EGF. We found that gefitinib promoted the loss of the EGF effect as it does not promote the formation of different clusters, both in the presence or absence of EGF (Fig. 4 F). Through heatmap analysis of intracellular metabolites, we observe that cells treated with gefitinib form a cluster isolated from the remaining clusters and it does not depend on EGF (Fig. 4 G).

Considering the heatmap from Fig. 4 E, showing the metabolites of PC-9 cells exposed to glucose, gefitinib, or lactate with or without EGF, it was observed that glucose and EGF decreased the levels of intracellular alanine, glycine, leucine, lysine, and tyrosine (Fig. 4 E, Supplementary Fig. 4 A). Controversially, these amino acids were also decreased by gefitinib, together with isoleucine, methionine, phenylalanine, threonine, and valine, and the tripeptide glutathione. Interestingly, glucose was only detected in cells exposed to gefitinib in the presence of glucose. Lactate-treated cells also showed reduced levels of alanine, and lactate plus EGF significantly increased the levels of glutathione. Both intracellular acetate and formate were increased in the presence of lactate (Fig. 4 E, Supplementary Fig. 4 B). Hypoxanthine was increased after lactate addition and uracil was also higher in the presence of lactate plus EGF (Fig. 4 E, Supplementary Fig. 4 C).

At the extracellular level, alanine, glutamate, acetate, and citrate tended to increase in glucose-treated cells exposed to EGF (Fig. 4 E, Supplementary Fig. 4 D, and E). Moreover, gefitinib increased the levels of glutamate and glutamine in the presence of glucose. Gefitinib in combination with EGF further enhanced glutamate, glutamine, glycine, isoleucine, leucine, lysine, and threonine. Regarding extracellular sugars and organic acids, it was found that gefitinib alone or in combination with EGF increased the levels of lactate in PC-9 cells exposed to glucose and tended to increase α-ketoglutarate levels (Fig. 4 E, Supplementary Fig. 4 E). In addition, gefitinib and gefitinib plus EGF promoted higher levels of uracil (Fig. 4 E, Supplementary Fig. 4 F). Lactate alone or in combination with EGF led to an increase in alanine, lysine, and valine extracellular levels (Fig. 4 E, Supplementary Fig. 4 E).

3.7. Lactate, independently of EGF, stimulates the expression of genes involved in lactate- and glucose-dependent pathways, which are in a cell line-dependent manner affected by gefitinib

The luciferase reporter gene assay showed that lactate with or without EGF increased MCT1 promoter activity; being the difference significant in H292 cells and in PC-9 a trend was observed (Fig. 5 A). Glucose in combination with EGF also significantly increased MCT1 promoter activity in PC-9 (Fig. 5 A). No meaningful differences were observed in A549 cells (Fig. 5 A).

The role of EGF in the regulation of gene expression in cells cultured in the presence and absence of glucose and lactate was evaluated by qPCR. It was observed that the presence of EGF did not interfere with the expression of most of the studied genes, being the observed modulation related to the lactate and glucose supplementation.

Firstly, genes involved in glucose and lactate transport, and lactate synthesis were analyzed. In the A549 cell line, the expression of *MCT1* and *MCT4* was stimulated by lactate and glucose (Fig. 5 B, Supplementary Fig. 5 A). In H292 cells, the same was observed considering the expression of *MCT1* (Fig. 5 B, Supplementary Fig. 5 A), while *MCT4* was overexpressed only upon exposure to lactate. In PC-9, the expression of *MCT1* remained unchanged amongst culture conditions; and *MCT4* expression was increased by lactate. Both *LDHA* and *LDHB* expression was significantly increased in all cell lines under lactate exposure (Fig. 5 B, Supplementary Fig. 5 A). In which concerns the glucose transporters, lactate stimulated the expression of both *GLUT1* and *SGLT1* in all cell lines (Fig. 5 B, Supplementary Fig. 5 B). *SGLT1* expression was decreased by glucose exposure in A549 cells (Fig. 5 B). Glucose led to higher levels of *SGLT1* expression in PC-9 cells (Fig. 5 B).

Considering the intracellular synthesis as a source of glucose, the expression of genes involved in gluconeogenesis was evaluated. The levels of *PEPCK* or *PCK1* mRNA are significantly increased in all cell lines in the presence of lactate (Fig. 5 B, Supplementary Fig. 5 C). In H292, lactate and lactate plus EGF increased the expression of *PCK2* in a significant manner while in PC-9 cells, only lactate alone exerted an increase in the expression of this gene. *ALT* gene encodes the alanine transaminase, which supplies gluconeogenesis as a source of pyruvate, and curiously lactate stimulated *ALT* expression in all cell lines.

Concerning the metabolic regulation of glucose degradation and synthesis, the expression of PFKFB1 was assessed, which is an activator of glycolysis and an inhibitor of gluconeogenesis. In H292 and PC-9 cells, lactate increased the expression of *PFKFB1*, (Fig. 5 B, Supplementary Fig. 5 D). The expression of *G6PD,* encoding the limiting enzyme of PPP, in H292 and PC-9 was increased by lactate , and glucose induced the opposite by decreasing *G6PD* expression in H292 and A549 cells.

Although the expression of most genes was independent of EGF presence, it was important to verify if EGFR activity was acting on these genes' expression. Therefore, the effect of gefitinib at the gene expression level was explored, and cells were exposed to gefitinib, alone or in combination with lactate or lactate plus EGF. Gefitinib abolished the lactate-mediated high expression of *MCT1*, *MCT4*, *LDHA*, *LDHB*, *GLUT1,* and *PEPCK*, in H292 and A549 cells (Fig. 5 C). In A549, G6PD expression increased with gefitinib treatment. A gefitinib-related expression profile was observed in PC-9 cells, revealing an increase in *MCT1*, *SGLT1*, *PEPCK,* and *ALT* and a decrease in *MCT4*, *LDHA*, *GLUT1,* and *PFKFB1* expression upon EGFR inhibition.

3.8. EGF in the presence of glucose or lactate interferes differently with the cell proliferation of NSCLC cells

To reinforce the effect of glucose availability and lactate usefulness in cell proliferation, assays were performed comparing the cell cycle dynamics of glucose and lactate culture conditions with no-glucose and no-glucose plus EGF control conditions. The presence of lactate increased the percentage of cells in the G0-G1 phase in A549 and H292

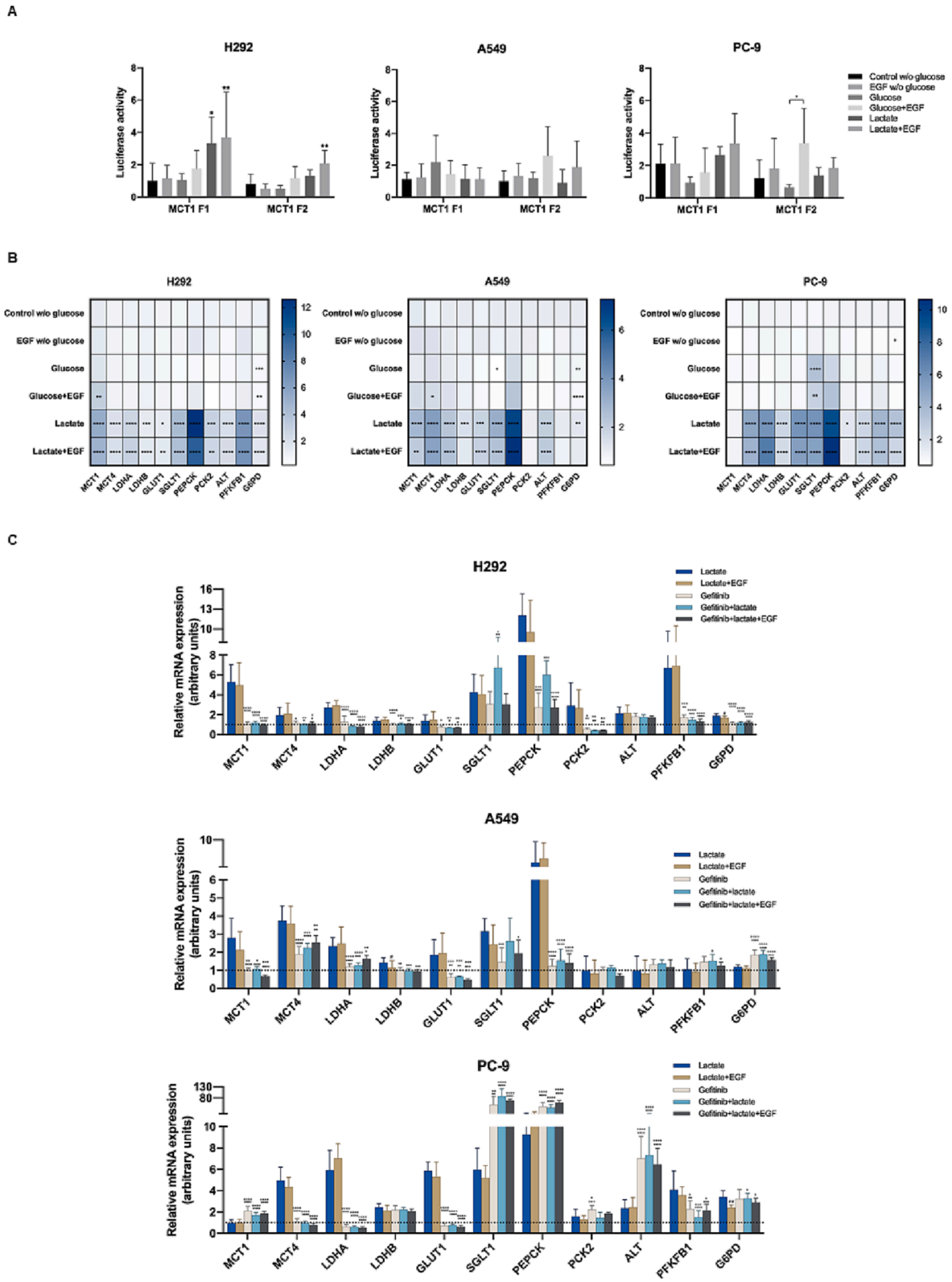

Fig. 5. Lactate alone or in combination with EGF promotes the activation of the MCT1 promoter in H292 and stimulates the expression of genes involved in lactate- and glucose-dependent pathways, which are affected by gefitinib in a cell line-dependent manner. Cells were cultured in control conditions, in the presence of glucose or lactate, and with EGF stimulation in the presence and absence of glucose/lactate. **(A)** Luciferase activity of MCT1 (F1 and F2) promoter constructs in transfected cells. **(B)** Heatmap showing the relative gene expression of relevant metabolic genes. **(C)** Relative gene expression of metabolic genes in cells cultured in control conditions (baseline culture medium represented by the dotted line), in the presence of gefitinib alone or in combination with lactate or lactate plus EGF. Results are shown as mean ± SD *$p < 0.05$, **$p < 0.01$, ***$p < 0.001$. One-way ANOVA with Dunnett's multiple comparisons test was used.

cells (Fig. 6 A), and the same was seen in A549 cells exposed to lactate and EGF. The lactate and glucose effect was observed in later time points, in A549 and H292, in which an increase in cell number was observed, independently of EGF (Fig. 6 B). In PC-9 exposed to lactate or glucose together with EGF, the percentage of cells in respectively G2/M and S phases was increased. The same was observed in cell counting, in which EGF increased the proliferation of lactate- treated PC-9 cells at 48 h.

We calculated the doubling time of each cell line in all experimental conditions (Table 2), and PC-9 showed the lowest cell doubling time and EGF tended to decrease the cell doubling time in all conditions in A549 and PC-9 cells. Glucose decreased the cell doubling time in H292 and A549 while lactate plus EGF decreased the cell doubling time in PC-9 cells. EGF tends to increase cell proliferation at 24 h and 32 h in PC-9.

Since the MAPK/ERK kinase and PI3K-Akt-mTOR pathways are known to be activated downstream of the EGFR, accounting for cancer cell proliferation [30], we analyzed the phosphorylation of ERK1/2 and

Table 2
Glucose decreases the cell doubling time in H292 and A549 while lactate plus EGF reduces the doubling time in PC-9 cells.

Cell line	Cell doubling time (h) Control	EGF	Glucose	Glucose + EGF	Lactate	Lactate + EGF
H292	22,4 ± 1,8	21,9 ± 2,2	19,03* ± 2,03	22,4 ± 2,2	20,9 ± 2,4	22,1 ± 1,8
A549	22,8 ± 3,02	20,3 ± 3,9	18,7* ± 3,6	16,3** ± 2,4	19,9 ± 3,3	18,7 ± 1,8
PC-9	21,96 ± 3,3	18,9 ± 3,9	21,09 ± 5,1	18,9 ± 4,1	17,45 ± 2,5	15,6** ± 3,4

Akt. Src protein is also a target of EGFR activation, being a player in proliferation and overactivated in cetuximab (KRAS blocker) resistant NSCLC [31], thus p-Src levels were assessed. ERK phosphorylation was stimulated by EGF, under glucose conditions, in H292 and PC-9 cells

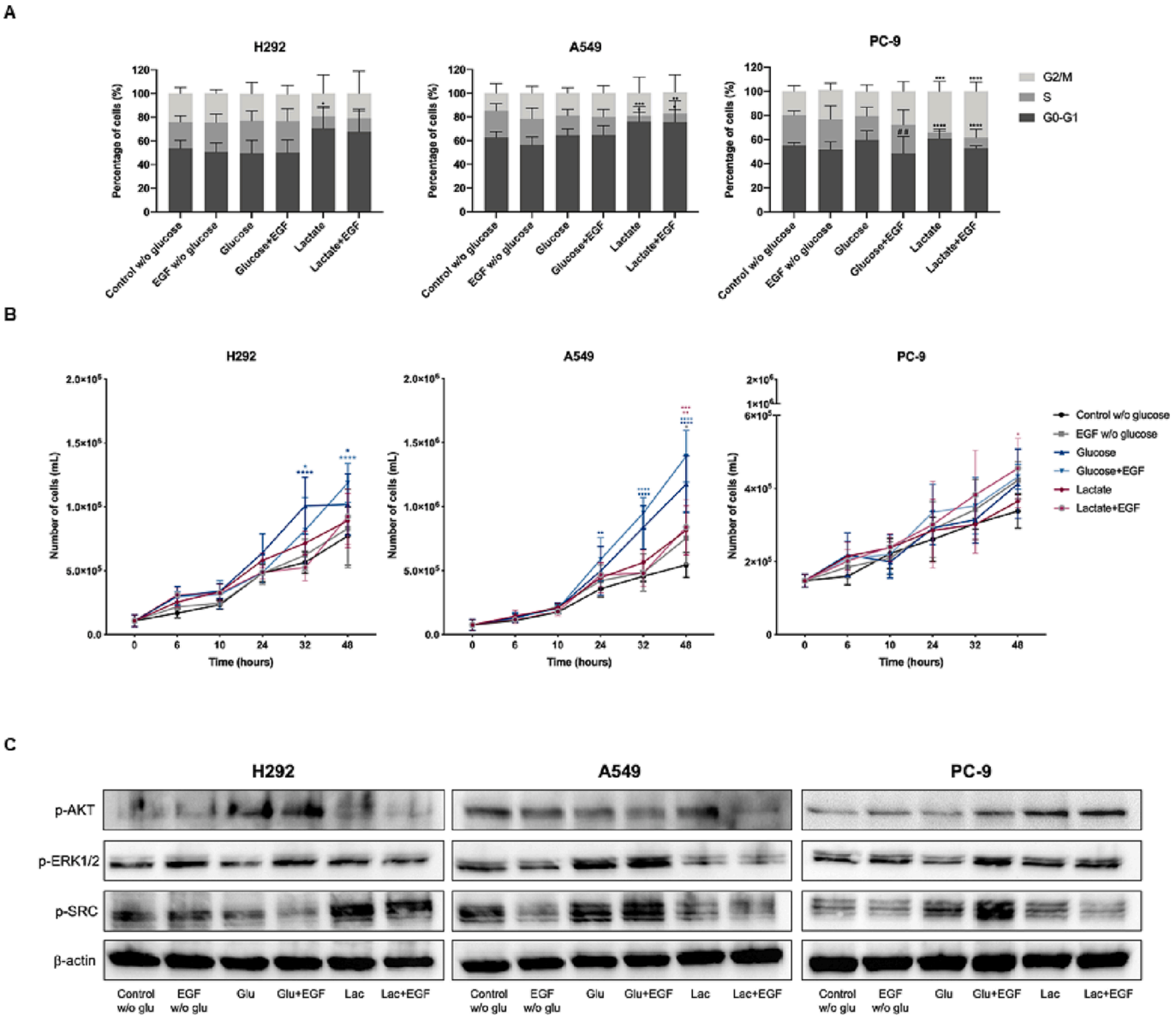

Fig. 6. EGF in the presence of glucose or lactate interferes differently with cell proliferation of NSCLC cells. Cells were cultured in control conditions, in the presence of glucose or lactate, and with EGF stimulation in the presence and absence of glucose/lactate. **(A)** Cell cycle analysis by flow cytometry (PI staining) and **(B)** proliferation curves in cells exposed to aforementioned conditions for 0, 6, 10, 24, 32, and 48 h. **(C)** Phosphorylation of AKT, ERK1/2, and SRC was analyzed using specific antibodies by western blotting. Results are shown as mean ± SD *p < 0.05, **p < 0.01, ***p < 0.001. Two-way ANOVA with Tukey's test or one-way ANOVA with Dunnett's multiple comparisons test was used.

(Fig. 6 C). p-AKT levels were higher in glucose conditions in H292 and in lactate conditions in PC-9 cells. In agreement, our previous results showed that lactate alone or in combination with EGF stimulated the cell cycle in PC-9 cells. Glucose with or without EGF strongly induced p-SRC in A549 cells, while in PC-9, p-Src levels increase with EGF stimulation in glucose-treated cells. Regarding H292 cells, increased p-Src levels were observed in H292 in the presence of lactate. Overall, PC-9 cells are the cells most responsive to EGF when they are in the presence of glucose.

3.9. *MCT1 and GLUT1 are positively correlated and upregulated in NSCLC metastatic samples*

The mRNA expression of relevant metabolic genes was evaluated in FFPE tumor samples from NSCLC patients.

In our cohort, the genes showing the highest levels of expression were *MCT4*, *LDHA,* and *LDHB* (Fig. 7 A). To investigate further associations in the expression of these genes, Spearman's correlation test was used and revealed a weak positive/direct correlation between *MCT1* and *MCT4* ($r_s = 0.41$), *GLUT1* and *LDHA* ($r_s = 0.48$) and *MCT4* and *LDHA* ($r_s = 0.37$) (Fig. 7 B). A weak negative/inverse correlation was also observed between *LDHA* and *SGLT1* ($r_s = -0.44$). A moderate positive/direct correlation was found between *MCT4* and *GLUT1* ($r_s = 0.52$), and *MCT1* and *GLUT1* ($r_s = 0.47$). *LDHA* and *LDHB* ($r_s = 0.69$) strongly correlated.

Interestingly, we found that *MCT1* and *GLUT1* mRNA levels were significantly higher in metastases comparing to primary tumors (Fig. 7 C). Additionally, adenosquamous tumors showed a higher expression of *MCT1* and *MCT4*, while squamous tumors had higher levels of *LDHA* and *LDHB* (Fig. 7 D).

Considering the mutational profile of the cohort included in this study, although in both primary tumors and metastases the most frequently mutated gene was *KRAS* followed by *EGFR*, only primary tumors harbored mutations in *BRAF* (Fig. 7 E). Regarding *EGFR* mutations present in all NSCLC tumors, the most frequent ones in this cohort were the L858R mutation (21.4%), and E746_A750del (21.4%). Gene expression analysis according to the different types of mutation was also performed in primary tumors and metastatic samples (Supplementary Fig. 6). Primary tumor samples harboring mutations in *BRAF*, *KRAS,* and *MET* exhibited upregulated *MCT4* expression when comparing to *EGFR*-mutated tumors. Concerning *GLUT1*, higher levels of this gene were detected in *KRAS* and *MET*-mutated primary tumors, contrasting with tumor samples bearing mutations in *EGFR*. Metastatic samples displayed an increased *GLUT1* mRNA expression comparing to *KRAS*-altered samples. In comparison to WT primary tumors, *MET* and *ROS1*-mutated tumors showed higher levels of *LDHA* expression. In addition, *MET*-altered tumors also exhibited enhanced levels of *LDHB*.

Using mRNA expression data only from patients with the *EGFR* E746_A750del mutation, which is the mutation found in PC-9 cells, Spearman's correlation test was performed (Fig. 7 F). Very strong negative/inverse correlations were observed between *MCT1* and *SGLT1* ($r_s = -0.97$), *MCT4* and *SGLT1*($r_s = -0.91$), *GLUT1* and *SGLT1* ($r_s = -0.91$), *MCT1* and *LDHB* ($r_s = -0.94$), *MCT4* and *LDHB* ($r_s = -0.94$) and *LDHB* and *GLUT1* ($r_s = -0.94$). On the other hand, very strong positive/direct correlations were also found, namely between *MCT1* and *GLUT1* ($r_s = 0.89$), *MCT4* and *GLUT1* ($r_s = 1$), and between *LDHB* and *SGLT1* ($r_s = 0.97$).

4. Discussion

A better understanding of putative oncogene activation and the pivotal metabolic pathways is highly relevant, since it may help to define new and more effective metabolism-based therapeutic approaches for NSCLC patients. *EGFR* has long been identified as an oncogenic driver of NSCLC [32], but its role in metabolic remodeling has only more recently been explored [33]. Under physiological conditions, *EGFR* activation in cells is strictly regulated to maintain tissue homeostasis, but in tumors, EGFR is often overexpressed and correlates with more aggressive phenotypes [32,34]. EGFR is a frequently overexpressed RTK in NSCLC due to amplification of the *EGFR* gene; additionally, the sustained production of EGFR ligands in the tumor microenvironment and mutations within *EGFR* itself can lead to constitutively activated receptor state [32,34,35]. EGFR overactivation is believed to promote intense downstream signaling, resulting in higher metastatic rates, poor tumor differentiation, and aggressive tumor behavior [32,36].

In this study, the role of *EGFR* status in metabolic profiling was explored considering glucose and lactate metabolism. It was shown that EGF stimuli exerted different effects on different NSCLC cell lines accounting for different metabolic profiles. Therefore, metabolic profiling may harbor details needed to distinguish NSCLC subsets, which in the future may benefit from more specific metabolism-based anti-cancer approaches. Indeed, PC-9 cells were the most responsive to EGF exposure, as this growth factor favored cell cycle progression and increased expression of *CCDN1* mRNA, encoding cyclin D1 (Fig. 1 B and C), an activator of CDK4 and CDK6 [37]. Cyclin D1 expression is regulated by AP-1, a transcription factor that acts as a response to external stimuli, activating MAPK and PI3K/AKT pathways [38,39]. In agreement, previous studies showed that blocking EGFR ligand binding by a monoclonal antibody or EGFR TKIs caused a cell cycle arrest reducing CDK activity from the G1 phase [40]. Moreover, the migration rate of PC-9 cells was significantly increased by EGF (Fig. 1D). A549 cells (KRAS p.G12S) also displayed enhanced migration upon EGF, at later time points. According to the literature, EGF was shown to induce migration in different cell models, being linked to epithelial-to-mesenchymal transition (EMT) [41], a mechanism described in A549 cells due to EGF stimulation [42]. Additionally, EGFR is known to activate matrix metalloproteinases (MMPs) which degrade the extracellular matrix (ECM), favoring cell motility and invasion, thereby connecting EGFR overactivity and metastatic potential [43,44]. Several studies demonstrated MMP-9 overexpressed under EGFR-dependent signaling, contributing to numerous metastatic steps in ovarian cancer [45] and in NSCLC [46]. Our findings are in agreement with the crucial role of *EGFR* in the control of NSCLC cell migration.

The expression of EGFR and HER2 in NSCLC cell lines was assessed to evaluate the different stimulation capacities of EGF on cancer cells. Amongst cell lines, it was observed a different expression pattern of these EGF receptors. EGF was able to upregulate the expression of EGFR and HER2 in PC-9 cells (Fig. 2 A, B, E, and F), which was not expected since the PC-9 cell line harbors the *EGFR* exon 19 E746-A750 deletion and should have the EGFR downstream pathways constitutively activated in an EGF-independent manner. However, considering that HER2 does not bind directly to any known ligands, but it heterodimerizes with ligand-activated EGFR or other family members [47,48], the presence of HER2 may promote the dimerization with EGFR upon EGF exposure and increase the response to EGF stimulus. Another possible explanation is the fact that PC-9 cells also express the WT variant of EGFR, as seen in Fig. 2 D, thus the stimulation by EGF can occur in the WT rather than in the mutated protein. Moreover, it was reported that EGF exposure to PC-9 cells induced EGFR phosphorylation at Y845 and Y1173, showing that the mutant receptors remained sensitive to ligand stimulation [49]. Looking at the immunofluorescence images (Fig. 2 A), EGFR localized in small agglomerates in the cytoplasm, resembling vesicle-like structures, and in clusters near the nucleus, especially in A549. This is in agreement with other studies using A549 [42] and PC-14 cells [50] (which are presently known as PC-9 cells).

Cancer cells strive to meet their optimal metabolic requirements in a TME marked by dynamic changes in nutrient availability [12]. High concentrations of metabolites in the TME, particularly lactate, contribute to all the main stages of carcinogenesis including angiogenesis, immune escape, cell migration, and metastasis [12,51]. An increasing number of studies has demonstrated that lactate is not only an

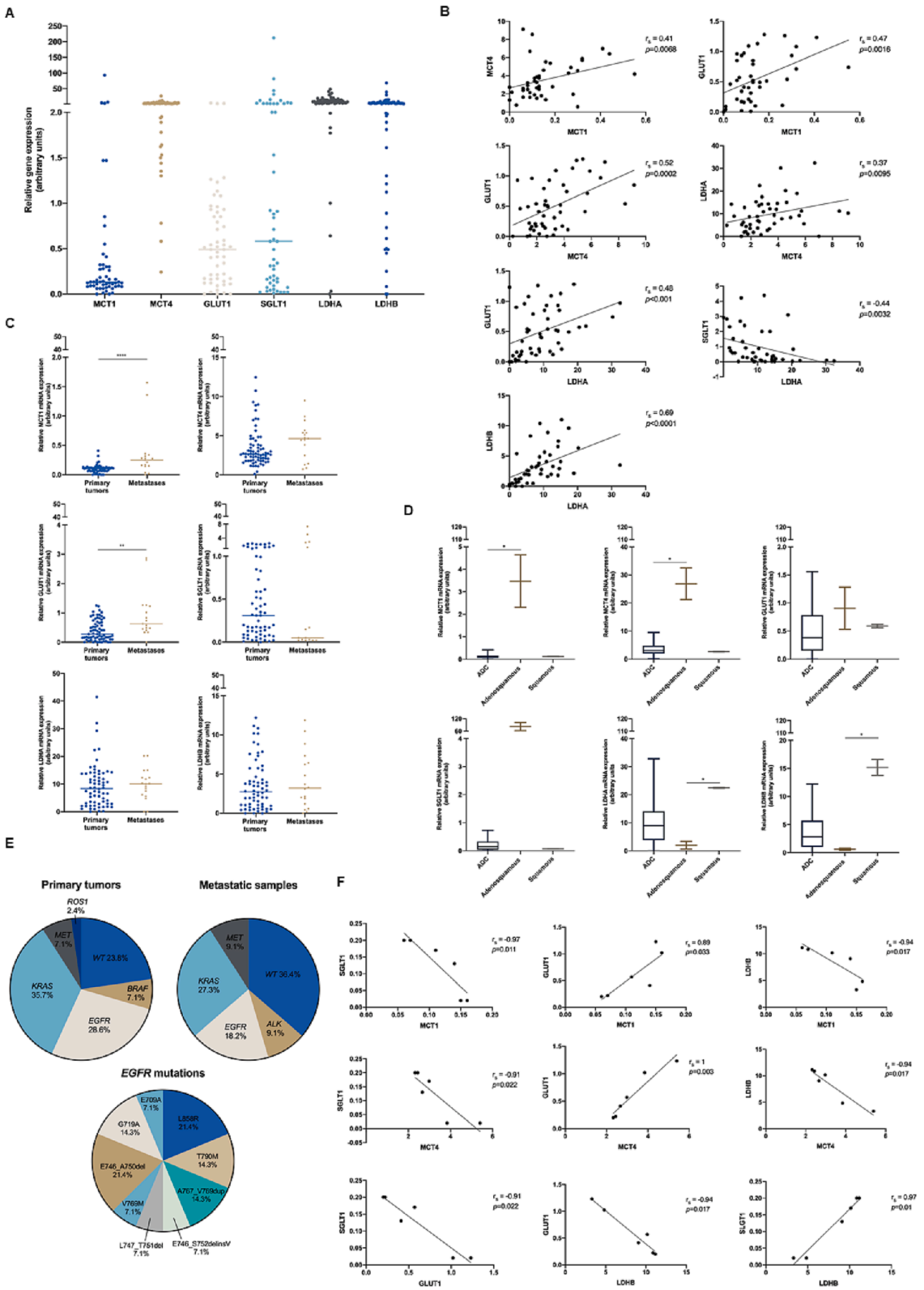

Fig. 7. ***MCT1*** **and** ***GLUT1*** **are positively correlated and upregulated in NSCLC metastatic samples and very strong direct correlations were found between** ***GLUT1*** **and** ***MCT1/MCT4*** **and** ***SLGT1*** **and** ***LDHB*** **in patients with the** ***EGFR*** **E746_A750del mutation. (A)** *MCT1*, *MCT4*, *GLUT1*, *SGLT1*, *LDHA*, and *LDHB* mRNA was quantified by relative quantifying real-time PCR using NSCLC patient samples. **(B)** Spearman's correlation analysis showing gene expression levels in NSCLC patients. Spearman's correlation coefficient (r_s) and p-values are shown for each analysis. **(C)** Analysis of gene expression profiles in **(C)** primary carcinomas and metastases and in **(D)** adenocarcinomas (ADC), adenosquamous, and squamous NSCLC samples. **(E)** Pie charts showing the percentage of mutations detected in primary tumors and metastatic tumors, as well as the frequency of the different *EGFR* mutations detected in NSCLC patient samples. **(F)** Spearman's correlation analysis using mRNA expression data from patients harboring the *EGFR* E746_A750del mutation. Results are shown as median. The asterisks (*) represent the statistical significance among groups. *p < 0.05, **p < 0.01, ***p < 0.001. Independent samples Kruskal Wallis One-way ANOVA with multiple comparisons or Mann-Whitney test.

end product of glycolysis, but also an important metabolic source for cancer cells [12] and a regulator, participating in several signaling pathways in normal and tumor tissue [52]. The transport of monocarboxylates such as lactate, pyruvate, and ketone bodies across the cell membrane is crucial for carbohydrate, fat, and amino acid metabolism and is facilitated by proton-linked monocarboxylates transporters (MCTs) 1–4 [53]. MCT1 and MCT4 have been considered the most relevant transporters in this process and are both able to import and export substrates, being MCT1 often associated with import and MCT4 with export [54,55]. Here, we found that EGF differently impacts the regulation of MCTs in NSCLC. MCT1 was upregulated by EGF in H292 and PC-9 cells, while MCT4 was only modulated in PC-9 (Fig. 3 A, B, F, G). The increasing expression of MCT1 was accompanied by a decrease in intracellular levels of lactate (Fig. 3 E), suggesting that lactate is probably being used as fuel. Faubert et al. showed in NSCLC patient–derived samples and in mouse models, that lactate was a major source for the TCA cycle, and MCT1 was the main intervenient in this context [11]. Moreover, Silva et al. [29] showed that the consumption of lactate could be a metabolic expertise of certain types of cancer cells, such as the squamous cells of the uterine ectocervix that can consume lactate from the cervicovaginal microenvironment [12]. In that study, they found that squamous carcinoma cells were well adapted to fully metabolize lactate, while adenocarcinoma cells, derived from glandular cells from the endocervix, were not able to consume lactate. Their findings were validated in tumor sections, showing that squamous carcinomas expressed preferentially MCT1 but adenocarcinomas expressed MCT4 [12,29]. In the present study, the cell line with the highest levels of MCT1 was H292 (Fig. 3A), which is from a squamous cell carcinoma histological subtype and was derived from a lymph node metastasis [56,57]. On the other hand, PC-9 cells were established from a lymph node of a lung adenocarcinoma [58,59] and highly expressed MCT4 (Fig. 3 F). A549 cells were isolated from an adenocarcinoma and show intermediate expression of MCT1 and low expression of MCT4. In NSCLC, it was also demonstrated that squamous cell carcinomas exhibited more active catabolism of glucose into different pathways including glycolysis, TCA cycle, and nucleotide, amino acid, and glutathione synthesis when comparing to adenocarcinomas [60]. Thus, it appears that metabolism may be differently reprogrammed in the major NSCLC subtypes and the way cancer cells metabolize lactate resembles a cell of origin-dependent expertise, in which MCT1 is pivotal.

Accordingly, the NSCLC cell lines used in this study showed different metabolic profiles (Fig. 4). The analysis of ^{1}H NMR spectra from culture media (extracellular metabolites) and aqueous intracellular metabolites revealed that lactate potentiated differences in the metabolic profile of each cell line (Fig. 4 A). The PCA scores of A549 and H292 intracellular metabolites in the presence of lactate overlap, suggesting the existence of similarities between A549 and H292 metabolism when the carbon source is lactate. However, PC-9 metabolic profile is different, indicating a different adaptation of this cell line to lactate metabolism. Additionally, in the multivariate analysis, the EGF stimulus did not affect H292 and A549 cells' metabolic profile, but it modulated PC-9 cells' metabolism (Fig. 4 B). Indeed, the PCA scores of intracellular extracts of PC-9 cells displayed a significant influence of EGF using glucose as a carbon source, forming different groups of cells exposed or not to EGF. Interestingly, this effect was lost when cells were treated with gefitinib, an EGFR TKI (Fig. 4 F and G). In PC-9, gefitinib treatment led to a decrease in glucose consumption (Fig. 4 E, Supplementary Fig. 4 B), suggesting that the abolition of EGFR signaling pathways affected the glycolytic rate. In agreement, gefitinib treatment is described as reducing glucose transporter 3 (GLUT3) levels in cancer cells' plasma membrane concomitant with the increased cytosolic levels, in lung cancer cell lines [61], suggesting that gefitinib increases the internalization of GLUT3, reducing glucose transport ability. A similar outcome was observed when a third-generation EGFR-TKI was employed in NSCLC [62].

As mentioned previously, PC-9 has an *EGFR*-activating mutation consisting of an in-frame deletion in exon 19 (EGFR$^{delE746\text{-}A750}$), which leads to structural changes and increased affinity interaction between ATP and EGFR over-activating the kinase domain [19]. Gefitinib is a competitive inhibitor of the tyrosine kinase-ATP binding site that alters EGFR tyrosine kinase activity and blocks downstream signaling pathways [20,21]. This inhibitor shows a higher affinity for EGFR with activating mutations [22] and since PC-9 cells show constitutive activation of the EGFR signaling pathway due to *EGFR*$^{delE746\text{-}A750}$, even in the absence of EGF, gefitinib still exerts its inhibitory effect, which leads to a different metabolic behavior from that shown in cells cultured with glucose alone.

In all cell lines, the glycolysis pathway was activated since in glucose-cultured cells, lactate was detected instead of glucose, indicating glucose catabolism. EGFR signaling activation has previously been linked to increased glycolysis activity in a variety of malignancies, including breast [63] and lung cancer [26]. However, the molecular mechanism by which EGFR signaling regulates glucose transport is still uncertain. EGFR was found to be physically associated with and stabilized the sodium/glucose transporter (SGLT1) to promote glucose uptake into cancer cells [64].

Looking in more detail at the metabolite concentrations in H292 cells (Fig. 4 C, Supplementary Fig. 2), results suggest that EGF stimulates lactate consumption to fuel the TCA cycle. This can be seen by the increase in the production of aspartate since aspartate and asparagine levels can indicate the synthesis of oxaloacetate, as in an aspartate-free medium oxaloacetate may be the sole source of aspartate [65]. Lactate also contributed to the synthesis of nitrogenous bases, such as purine synthesis (guanosine and inosine) and pyrimidine (cytidine). These findings are in agreement with the MCT1 expression profile, showing that lactate alone or in combination with EGF stimulates the activation of the MCT1 promoter and gene expression (Fig. 5 A and B). Glutamine catabolism is increased in A549 cells since no glutamine was detected in intracellular extracts, suggesting that it was catabolized in glutamate (Fig. 4 D, Supplementary Fig. 3 A). Accordingly, glutamate and succinate levels were increased in cells exposed to glucose and EGF. Excess glutamate is probably being converted into succinate as well as alanine, which is also augmented in the presence of glucose plus EGF. Additionally, glutamine-derived glutamate also donates its amine nitrogen toward the biosynthesis of serine and consequently the synthesis of glycine [66]. Glutamine was found to be a crucial source for bioenergetics and biosynthesis in *EGFR*-mutated NSCLC and the combinatory treatment of erlotinib with a glutaminase inhibitor (CB-839) increased the levels of cell death and resulted in tumor regression in mouse NSCLC xenografts [67]. In addition, glutamate can be transported through the xCT antiporter in exchange for cystine, which is quickly reduced to cysteine inside the cell [68]. This may explain the presence of cysteine in A549 intracellular extracts. These results are in agreement with other studies, as the involvement of mutant *KRAS* in the metabolic rewiring with increased glutamine utilization was reported in different types of cancer [17,18]. In PC-9 cells, EGF increased the consumption of alanine, leucine, lysine, phenylalanine, and tyrosine; and gefitinib decreased the consumption of glucose and the levels of several intracellular amino acids. Thus, in this scenario, it is probable that the glucose-treated cells used intermediates of the glycolytic pathway as precursors for the synthesis of amino acids. On the other hand, PC-9 treated with gefitinib showed, on growth media, higher levels of aspartate and glutamate, which is a precursor of α-ketoglutarate and the main spot of entrance of glutamine-derived compounds in the TCA cycle [69,70]. This observation, together with the trend to increase α-ketoglutarate levels (Supplementary Fig. 4) suggests that glucose is accounting for the production of TCA cycle intermediates, and glutamine metabolism is originating amino acids, which may be used by the cell to support pivotal metabolic pathways. Accordingly, glutamine-derived aspartate has been described as crucial for nucleotide biosynthesis and redox control in cancer cells [71]. Moreover glutamate export more commonly occurs upon cyst(e)ine import [72], a crucial metabolic player in carbon and energy metabolism as well as a component of

glutathione, supporting the high metabolic flow and chemoresistance. As mentioned, cysteine was not detected within the PC-9 cells, but glutathione turnover is highlighted by our results since reduced glutathione presents accentuated intracellular decreased levels upon gefitinib exposure. The results obtained through NMR spectroscopy are in line with the findings in Fig. 6, in which it is observed that NSCLC cell lines can adapt to environments lacking glucose as well as to exogenous lactate. The main conclusions of this study are schematically integrated in Fig. 8, identifying the main pathways acting on the NSCLC *in vitro* models explored (Fig. 8 A). Moreover, a feed-forward loop can be established between glucose and lactate consumption, in which the increased rate of glycolysis promotes increased lactate production which will stimulate cells to export transiently lactate and further control its import to sustain metabolic requirements. The higher the glycolysis rate is the higher lactate consumption will be (Fig. 8 B). Ultimately, different genetic patterns seem to condition the metabolic profiles (Fig. 8 C), highlighting that the metabolic definition may be a powerful tool to identify patients who may benefit from metabolism targeted-therapies as a strategy to surpass the expected mechanisms of resistance upon genetic-based targeted-therapy.

The role of EGF in the regulation of gene expression in cells cultured in the presence and absence of glucose and lactate was evaluated, evidencing that lactate bioavailability influenced the expression of several metabolic genes (Fig. 5 B and Supplementary Fig. 5). While EGF promoted an increase in MCT1 protein expression in H292 and PC-9, and MCT4 in PC-9 cells, at basal levels, the same was not observed at the mRNA level. Only H292 and A549 cells showed, respectively, augmented MCT1 and MCT4 expression after EGF exposure (Fig. 5 B, Supplementary Fig. 5 A). Lactate had a more prominent effect in the regulation of transcriptional activity of lactate and glucose-related transporters, but also of gluconeogenesis and PPP-related genes (Fig. 5 B). Indeed, lactate is actively exchanged to provide an oxidative energy source and gluconeogenic precursor [73] as well as for cell signaling [74], having been reported as a "lactormone" [12,75]. Besides, in a study using MCF7 cells, lactate influenced the gene expression of several key oncogenes and other driver genes involved in metabolic reprogramming, regulation of cell cycle, and proliferation [76]. Moreover, Zhang et al., [77] reported that "lactylation" of histone lysine residues acts as an epigenetic modification that directly induces gene transcription from chromatin in human and mouse cells. After exogenous lactate exposure, lysine lactylation (Kla) levels increased in a dose-dependent manner and endogenous production of lactate was a crucial driver of histone Kla levels [77]. Regarding gluconeogenesis, it was reported that NSCLC cells utilized this pathway to overcome glucose deprivation, a consequence of the high glucose consumption, and that PCK2 was expressed and active in NSCLC cell lines and samples [78]. In our study, we also found that lactate could serve as a gluconeogenic precursor, as *PEPCK* was significantly upregulated in all cell lines, and *PCK2* was enhanced in H292 cells, after lactate exposure (Fig. 5 B, Supplementary Fig. 5 C). PEPCK, which converts oxaloacetate (OAA) to phosphoenolpyruvate (PEP), has an important role in glucose production, but also in the generation of glycerol and serine [78]. PCK2, the mitochondrial isoform of PEPCK, was shown to directly influence TCA cycle function in cancer cells by catabolizing OAA generated from glutamine [79]. In an elegant study by Jin et al., [25] EGFR activation branched glycolysis to the serine synthesis for nucleotide biosynthesis and redox homeostasis. Interestingly, *PEPCK* expression was significantly upregulated in PC-9 cells exposed to lactate plus EGF (Supplementary Fig. 5 C), and through NMR, it was possible to see that serine production tended to be higher in lactate-treated cells (Fig. 4 E, Supplementary Fig. 4 A). Glutathione synthesis was also enhanced in these conditions, possibly contributing to redox homeostasis. Again, PPP can play a role in cancer cells' metabolic balance, since it is a glucose-dependent pathway, which can benefit from lactate as a gluconeogenesis substrate to contribute to nucleotide synthesis on one hand and to the regeneration of glutathione and redox control in another hand [80]. Accordingly, in our study *G6PD* gene is upregulated by lactate in PC-9 cells, being this effect rescued by EGFR blockade, as it will be further discussed.

The effect of gefitinib at the gene expression level was investigated alone or in combination with lactate or lactate plus EGF, evidencing that EGFR blockade promoted alterations in the expression profile of metabolism-related genes. Interestingly, PC-9 cells responded differently to gefitinib treatment when comparing to H292 and A549. Gefitinib abolished the expression of almost all genes studied in the *EGFR* WT cells, including glucose and lactate transporters, but also gluconeogenic and PPP genes. However, in PC-9 cells, *MCT1*, *SGLT1*, *PEPCK,* and *ALT* gene expression was upregulated by this TKI inhibitor (Fig. 5 C). This might be explained by the increased availability of glucose, as gefitinib decreased the consumption of glucose in these cells (Fig. 4 E, Supplementary Fig. 4 B). These findings cast doubt on whether patients with *EGFR* wild-type NSCLC may benefit from gefitinib therapy, or if an undisclosed mechanism of resistance to targeted therapy may be connected to metabolic remodeling, through which the adjustment of crucial bioenergetics and biosynthetic pathways strengthen cancer cells to overcome EGFR inhibition and increase their survival.

EGF induced the activation of MAPK/ERK and SRC pathways in all cell lines (Fig. 6 C). Interestingly, in the absence of glucose or upon lactate exposure, increased levels of p-Src were observed in H292. Although EGFR is activated through ligand binding and autophosphorylation of its cytoplasmic tail, it is well known that Src, or Src family kinases, are required for the full activation of EGFR [81]. It was reported that HER2 and Src mediated tyrosine phosphorylation of LDHA at tyrosine 10, activating LDHA and providing an anti-anoikis, pro-invasive and pro-metastatic potential to cancer cells [82]. Lactate was shown to upregulate SRC kinase activity, resulting in LDHA phosphorylation at Y10, triggering the transcriptional expression of VEGF under normoxia and Inducible Nitric Oxide Synthase (INOS) under hypoxia, to regulate macrophage polarization [83]. As H292 cells are metastatic, lactate may activate Src to further support the pro-metastatic potential of these cells. In future assays, it would be interesting to test the effect of gefitinib on molecular markers of the EGFR signaling cascade.

The analysis of NSCLC patients' mRNA showed significant positive correlations between *GLUT1* and *MCT1/4* and between *LDHB* and *SGLT1* in NSCLC patients harboring the *EGFR* E746_A750del mutation (Fig. 7 F). Additionally, both *MCT1* and *GLUT1* were upregulated in NSCLC metastatic samples (Fig. 7 C). A significant correlation between increased GLUT1, MCT1 mRNA levels/protein expression, and a high Fuhrman grade, the grading system used to predict survival for patients with renal cell carcinoma, was reported in clear-cell renal cell carcinoma patients [64]. Moreover, in this study, high *MCT1* and *GLUT1* mRNA levels correlated with poor prognosis, being revealed as strong prognostic markers and promising therapeutic targets in renal carcinoma context [64]. Several studies have suggested that NSCLC patients carrying the variant E746_A750del have a higher percentage of acquired T790M mutation than those with other *EGFR* 19Del variants following progression on earlier-generation TKIs [84–86]. The *EGFR* T790M mutation is recognized as the main mechanism of first/second-generation EGFR-TKI resistance [87]. Thus, NSCLC patients harboring the *EGFR* E746_A750del mutation are more prone to develop resistance to TKIs. In this context, considering the metabolic adaptation (Fig. 8 A) and combining GLUT1 inhibitors with MCT1/4 inhibitors, or inhibiting LDHB and SGLT1, could be an interesting therapeutic strategy to overcome the resistance in this specific group of NSCLC patients or at least these genes can be validated as markers for follow-up and prediction of therapy resistance. MCT1 inhibitor AZD3965 is in phase 1 clinical trials in patients with solid tumors and was already shown to be effective, especially in combined therapy [88]. Although no GLUT1 or MCT4 specific inhibitors have been advanced to clinical studies, several compounds have been identified as having an inhibitory effect [89,90]. Interestingly, *GLUT1* expression and glucose uptake were found to be increased in resistant NSCLC cells after treatment with gefitinib and

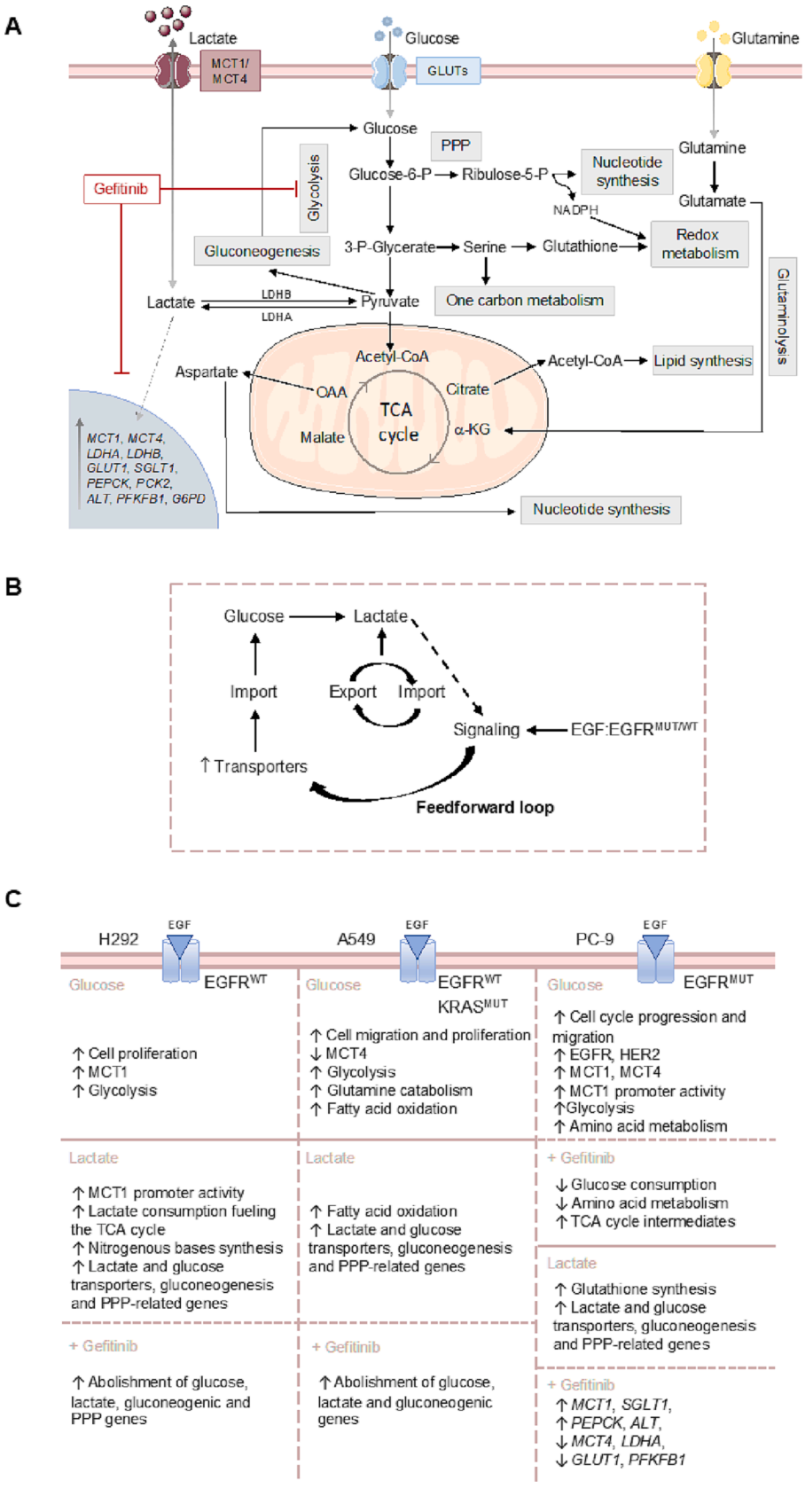

Fig. 8. NSCLC cell lines with different genetic profiles have heterogeneous metabolic specificities. (A) Schematic representation of the altered metabolic pathways in NSCLC. NSCLC cell lines exhibit an increased rate of glycolysis, which is hindered by gefitinib, at least in PC-9 cells. Glycolytic intermediates can supply PPP and one-carbon metabolism, promoting nucleotide and protein biosynthesis, which support cell growth and proliferation. The high glycolysis rate increases pyruvate levels that are converted into lactate by LDHA and exported by MCT4. Cancer cells are also known to consume lactate as a fuel; they import lactate through MCT1, which is converted into pyruvate by LDHB to sustain OXPHOS. Mitochondrial TCA cycle intermediates such as OAA and citrate can be used to generate aspartate and acetyl-CoA for nucleotide and lipid synthesis, respectively. NADPH and glutathione are essential to maintain cellular redox homeostasis. Fig. 8 C shows which metabolic pathways were increased in each NSCLC cell line studied here. Lactate alone or in combination with EGF stimulated the expression of genes involved in lactate- and glucose-dependent pathways, which are affected by gefitinib in a cell line-dependent manner. **(B)** Feed-forward loop can be established between glucose and lactate consumption. An increased rate of glycolysis promotes lactate bioavailability, which is managed by cancer cells to supply metabolic pathways with lactate-derived compounds. The phenotypical changes occurring in this scenario will prompt the maintenance of the high rate of glucose consumption to feed glucose-dependent and lactate-dependent biosynthesis and bioenergetics. **(C)** Main conclusions found in *EGFR*^{WT} H292, *EGFR*^{WT}, *KRAS*^{MUT} A549, and *EGFR*^{MUT} PC-9 cells exposed to EGF and glucose/lactate, in the presence or absence of gefitinib. ↓—decrease; ↑—increase. Glucose-6-P: glucose-6-phosphate; 3-P-Glycerate: 3-phosphoglycerate; R5P: ribulose 5-phosphate; OAA: oxaloacetate; α-KG: alpha ketoglutarate; MCT1/4: monocarboxylate transporter 1/4; LDHA/B: Lactate dehydrogenase A/B; GLUT1: Glucose transporter 1; SGLT1: Sodium/glucose cotransporter 1; PEPCK: Phosphoenolpyruvate carboxykinase; PCK2: Phosphoenolpyruvate Carboxykinase 2; ALT: Alanine transaminase; PFKFB1: 6-Phosphofructo-2-Kinase/Fructose-2,6-Biphosphatase 1; G6PD: glucose-6-phosphate dehydrogenase.

genetic or pharmacological inhibition of GLUT1 sensitized NSCLC with primary resistance and acquired resistance to gefitinib [91].

This study shows that both NSCLC cell lines and patient samples (Fig. 8 B and C) show heterogeneous metabolic profiles and are putatively associated with a particular genetic profile conditioning metabolic adaptation, potentially guiding patient stratification in innovative metabolism-targeted therapies in the scope of personalized medicine. It also reinforces that besides the complexity imposed by oncogenic alterations, one must consider the dynamic extrinsic factors which profoundly influence the metabolic adaptation of cancer cells. The metabolic specificities may enclose the necessary information to identify, distinguish and act effectively in the various subgroups of NSCLC, thus bringing an improvement in the therapeutic approach and outcome.

Ethical approval

The project and the use of NSCLC samples in the context of the mutation analysis performed for clinical management according to standard guidelines was approved by IPOLFG Ethical Committee (Ref: UIC/1442).

6. Authors' contributions

CM- wrote the 1st draft of the paper, planned and performed the most experiments, revised and discussed the paper; IL- performed NMR analysis, revised and discussed the paper; IF- performed NGS analysis, revised and discussed the paper; TA- responsible for clinical management of patients, revised and discussed the paper; FC- responsible for the pathology analysis of NSCLC, revised and discussed the paper; CA- coordinated NGS analysis, revised and discussed the paper; LGG- coordinated NMR spectroscopy analysis, revised and discussed the paper; JS- coordinated and supervised whole the project, responsible for getting funding, revised and discussed the paper.

Funding

The institutions are funded by Fundação para a Ciência e Tecnologia/Ministério da Ciência, Tecnologia e Ensino Superior (FCT/MCTES, Portugal) through national funds to iNOVA4Health (UIDB/04462/2020 and UIDP/04462/2020), to MOSTMICRO-ITQB (UIDB/04612/2020 and UIDP/04612/2020) and the Associated Laboratory LS4FUTURE (LA/P/0087/2020). Cindy Mendes was funded by a FCT individual Ph.D. fellowship (2020.06956.BD). Luis G. Gonçalves was financed by a FCT contract according to DL57/2016, [SFRH/BPD/111100/2015]. This work benefited from access to CERMAX, ITQB-NOVA, Oeiras, Portugal with equipment funded by FCT, project AAC 01/SAICT/2016.

8. Availability of data and materials

Metabolomics data will be made available in a public repository.

Declaration of Competing Interest

The authors declare that they have no known competing financial interests or personal relationships that could have appeared to influence the work reported in this paper.

References

[1] D. Planchard, S. Popat, K. Kerr, S. Novello, E.F. Smit, C. Faivre-Finn, T.S. Mok, M. Reck, P.E. Van Schil, M.D. Hellmann, S. Peters, Metastatic non-small cell lung cancer: ESMO Clinical Practice Guidelines for diagnosis, treatment and follow-up, Ann. Oncol. 29 (2018) iv192–iv237.

[2] L. Esposito, D. Conti, R. Ailavajhala, et al., Lung cancer: are we up to the challenge? Curr. Genomics 11 (2010) 513, https://doi.org/10.2174/138920210793175903.

[3] J.J. Lin, A.T. Shaw, Resisting resistance: targeted therapies in lung cancer, Trends Cancer 2 (7) (2016) 350–364.

[4] D. Hanahan, R.A. Weinberg, Hallmarks of cancer: The next generation, Cell 144 (2011) 646–674, https://doi.org/10.1016/j.cell.2011.02.013.

[5] C. Schiliro, B.L. Firestein, Mechanisms of Metabolic Reprogramming in Cancer Cells Supporting Enhanced Growth and Proliferation, Cells 10 (2021) 1056, https://doi.org/10.3390/CELLS10051056.

[6] J. Serpa, Metabolic Remodeling as a Way of Adapting to Tumor Microenvironment (TME), a Job of Several Holders, Adv. Exp. Med. Biol. 1–34 (2020), https://doi.org/10.1007/978-3-030-34025-4_1.

[7] H.MG. Vander, R.J. Deberardinis, Understanding the Intersections between Metabolism and Cancer Biology, Cell 168 (2017) 657–669, https://doi.org/10.1016/j.cell.2016.12.039.

[8] A. Hipólito, C. Mendes, J. Serpa, The Metabolic Remodelling in Lung Cancer and Its Putative Consequence in Therapy Response, Adv. Exp. Med. Biol. 1219 (2020) 311–333, https://doi.org/10.1007/978-3-030-34025-4_16.

[9] J.C. García-Cañaveras, A. Lahoz, Tumor Microenvironment-Derived Metabolites: A Guide to Find New Metabolic Therapeutic Targets and Biomarkers, Cancers (Basel) 13 (2021) 3230, https://doi.org/10.3390/CANCERS13133230.

[10] C. Hensley, B. Faubert, Q. Yuan, N. Lev-Cohain, E. Jin, J. Kim, L. Jiang, B. Ko, R. Skelton, L. Loudat, M. Wodzak, C. Klimko, E. McMillan, Y. Butt, M. Ni, D. Oliver, J. Torrealba, C. Malloy, K. Kernstine, R. Lenkinski, R. DeBerardinis, Metabolic Heterogeneity in Human Lung Tumors, Cell 164 (4) (2016) 681–694.

[11] B. Faubert, K.Y. Li, L. Cai, C.T. Hensley, J. Kim, L.G. Zacharias, C. Yang, Q.N. Do, S. Doucette, D. Burguete, H. Li, G. Huet, Q. Yuan, T. Wigal, Y. Butt, M. Ni, J. Torrealba, D. Oliver, R.E. Lenkinski, C.R. Malloy, J.W. Wachsmann, J.D. Young, K. Kernstine, R.J. DeBerardinis, Lactate Metabolism in Human Lung Tumors, Cell 171 (2) (2017) 358–371.e9.

[12] C. Mendes, J. Serpa, Revisiting lactate dynamics in cancer—a metabolic expertise or an alternative attempt to survive? J. Mol. Med. 98 (2020) 1397–1414, https://doi.org/10.1007/s00109-020-01965-0.

[13] Boidot R, Végran F, Meulle A, et al (2012) Regulation of monocarboxylate transporter MCT1 expression by p53 mediates inward and outward lactate fluxes in tumors. Cancer Res. 72:939–948. https://doi.org/10.1158/0008-5472.CAN-11-2474.

[14] Sonveaux P, Végran F, Schroeder T, et al (2008) Targeting lactate-fueled respiration selectively kills hypoxic tumor cells in mice. J. Clin. Invest. 118: 3930–3942. https://doi.org/10.1172/JCI36843.

[15] S. Hui, J.M. Ghergurovich, R.J. Morscher, C. Jang, X. Teng, W. Lu, L.A. Esparza, T. Reya, Le Zhan, J. Yanxiang Guo, E. White, J.D. Rabinowitz, Glucose feeds the TCA cycle via circulating lactate, Nature 551 (7678) (2017) 115–118.

[16] E. Kempf, B. Rousseau, B. Besse, L. Paz-Ares, KRAS oncogene in lung cancer: focus on molecularly driven clinical trials, Eur. Respir. Rev. 25 (2016) 71–76, https://doi.org/10.1183/16000617.0071-2015.

[17] J.R. Mayers, M.E. Torrence, L.V. Danai, T. Papagiannakopoulos, S.M. Davidson, M. R. Bauer, A.N. Lau, B.W. Ji, P.D. Dixit, A.M. Hosios, A. Muir, C.R. Chin, E. Freinkman, T. Jacks, B.M. Wolpin, D. Vitkup, M.G. Vander Heiden, Tissue of origin dictates branched-chain amino acid metabolism in mutant Kras-driven cancers, Science 353 (6304) (2016) 1161–1165.

[18] K.L. Bryant, J.D. Mancias, A.C. Kimmelman, C.J. Der, KRAS: Feeding pancreatic cancer proliferation, Trends Biochem. Sci. 39 (2014) 91–100, https://doi.org/10.1016/j.tibs.2013.12.004.

[19] H.Y. Min, H.Y. Lee, Oncogene-driven metabolic alterations in cancer, Biomol. Ther. 26 (2018) 45–56, https://doi.org/10.4062/biomolther.2017.211.

[20] R.A. Cairns, I.S. Harris, T.W. Mak, Regulation of cancer cell metabolism, Nat. Rev. Cancer 11 (2011) 85–95, https://doi.org/10.1038/nrc2981.

[21] P. Wee, Z. Wang, Epidermal growth factor receptor cell proliferation signaling pathways, Cancers (Basel) 9 (2017) 52, https://doi.org/10.3390/cancers9050052.

[22] A. Tomas, C.E. Futter, E.R. Eden, EGF receptor trafficking: Consequences for signaling and cancer, Trends Cell Biol. 24 (2014) 26–34, https://doi.org/10.1016/j.tcb.2013.11.002.

[23] Z. Zhang, A.L. Stiegler, T.J. Boggon, S. Kobayashi, EGFR-mutated lung cancer : a paradigm of molecular oncology, Oncotarget 1 (2010) 497–514.

[24] Z. Luo, M. Zang, W. Guo, AMPK as a metabolic tumor suppressor: Control of metabolism and cell growth, Futur. Oncol. 6 (2010) 457–470, https://doi.org/10.2217/fon.09.174.

[25] N. Jin, A. Bi, X. Lan, J. Xu, X. Wang, Y. Liu, T. Wang, S. Tang, H. Zeng, Z. Chen, M. Tan, J. Ai, H. Xie, T. Zhang, D. Liu, R. Huang, Y. Song, E.-H. Leung, X. Yao, J. Ding, M. Geng, S.-H. Lin, M. Huang, Identification of metabolic vulnerabilities of receptor tyrosine kinases-driven cancer, Nat. Commun. 10 (1) (2019), https://doi.org/10.1038/s41467-019-10427-2.

[26] H. Makinoshima, M. Takita, S. Matsumoto, A. Yagishita, S. Owada, H. Esumi, K. Tsuchihara, Epidermal growth factor receptor (EGFR) signaling regulates global metabolic pathways in EGFR-mutated lung adenocarcinoma, J. Biol. Chem. 289 (30) (2014) 20813–20823.

[27] K. Mizutani, X. Guo, A. Shioya, J. Zhang, J. Zheng, N. Kurose, H. Ishibashi, N. Motono, H. Uramoto, S. Yamada, The impact of PRDX4 and the EGFR mutation status on cellular proliferation in lung adenocarcinoma, Int. J. Med. Sci. 16 (9) (2019) 1199–1206.

[28] J. Serpa, P. Mesquita, N. Mendes, C. Oliveira, R. Almeida, F. Santos-Silva, C.A. Reis, J. LePendu, L. David, Expression of Lea in gastric cancer cell lines depends on FUT3 expression regulated by promoter methylation, Cancer Lett. 242 (2) (2006) 191–197.

[29] L.S. Silva, L.G. Goncalves, F. Silva, G. Domingues, V. Maximo, J. Ferreira, E.-F. Lam, S. Dias, A. Felix, J. Serpa, STAT3:FOXM1 and MCT1 drive uterine cervix

carcinoma fitness to a lactate-rich microenvironment, Tumor Biol. 37 (4) (2016) 5385–5395.
[30] W. Pao, J. Chmielecki, Rational, biologically based treatment of EGFR-mutant non-small-cell lung cancer, Nat. Rev. Cancer 10 (2010) 760–774, https://doi.org/10.1038/NRC2947.
[31] D.L. Wheeler, M. Iida, T.J. Kruser, M.M. Nechrebecki, E.F. Dunn, E.A. Armstrong, S. Huang, P.M. Harari, Epidermal growth factor receptor cooperates with Src family kinases in acquired resistance to cetuximab, Cancer Biol. Ther. 8 (8) (2009) 696–703.
[32] Herbst RS (2004) Review of epidermal growth factor receptor biology. Int. J. Radiat. Oncol. Biol. Phys. 59:S21–S26. https://doi.org/10.1016/j.ijrobp.2003.11.041.
[33] C. Mendes, J. Serpa, Metabolic remodelling: An accomplice for new therapeutic strategies to fight lung cancer, Antioxidants 8 (2019) 1–25, https://doi.org/10.3390/antiox8120603.
[34] T. Sasaki, K. Hiroki, Y. Yamashita, The role of epidermal growth factor receptor in cancer metastasis and microenvironment, Biomed. Res. Int. 2013 (2013) 1–8.
[35] N. Normanno, A. De Luca, C. Bianco, L. Strizzi, M. Mancino, M.R. Maiello, A. Carotenuto, G. De Feo, F. Caponigro, D.S. Salomon, Epidermal growth factor receptor (EGFR) signaling in cancer, Gene 366 (1) (2006) 2–16.
[36] T. Mukohara, S. Kudoh, S. Yamauchi, et al., Expression of epidermal growth factor receptor (EGFR) and downstream-activated peptides in surgically excised non-small-cell lung cancer (NSCLC), Lung Cancer 41 (2003) 123–130, https://doi.org/10.1016/S0169-5002(03)00225-3.
[37] S. Qie, J.A. Diehl, Cyclin D1, Cancer Progression and Opportunities in Cancer Treatment, J. Mol. Med. (Berl) 94 (12) (2016) 1313–1326.
[38] H. Gazon, B. Barbeau, J.M. Mesnard, J.M. Peloponese, Hijacking of the AP-1 signaling pathway during development of ATL, Front. Microbiol. 8 (2018) 2686, https://doi.org/10.3389/FMICB.2017.02686/BIBTEX.
[39] Y. He, M.M. Sun, G.G. Zhang, J. Yang, K.S. Chen, W.W. Xu, B. Li, (2021) Targeting PI3K/Akt signal transduction for cancer therapy, Signal Transduct. Target. Ther. 6 (1) (2021), https://doi.org/10.1038/s41392-021-00828-5.
[40] X. Wu, M. Rubin, Z. Fan, T. DeBlasio, T. Soos, A. Koff, Jm,, Involvement of p27KIP1 in G1 arrest mediated by an anti-epidermal growth factor receptor monoclonal antibody - PubMed, Oncogene 12 (1996) 1397–1403.
[41] J.P. Thiery, Epithelial–mesenchymal transitions in tumour progression, Nat. Rev. Cancer 2 (2002) 442–454, https://doi.org/10.1038/nrc822.
[42] C. Lauand, P. Rezende-Teixeira, B.A. Cortez, E.L.d.O. Niero, G.M. Machado-Santelli, Independent of ErbB1 gene copy number, EGF stimulates migration but is not associated with cell proliferation in non-small cell lung cancer, Cancer Cell Int. 13 (1) (2013), https://doi.org/10.1186/1475-2867-13-38.
[43] M. Ramírez Moreno, N.A. Bulgakova, The Cross-Talk Between EGFR and E-Cadherin, Front. Cell Dev. Biol. 9 (2021), https://doi.org/10.3389/FCELL.2021.828673.
[44] S.G. Da Cunha, F.A. Shepherd, M.S. Tsao, EGFR mutations and lung cancer, Annu. Rev. Pathol. 6 (2011) 49–69, https://doi.org/10.1146/ANNUREV-PATHOL-011110-130206.
[45] S.M. Ellerbroek, J.M. Halbleib, M. Benavidez, et al., Phosphatidylinositol 3-kinase activity in epidermal growth factor-stimulated matrix metalloproteinase-9 production and cell surface association, Cancer Res. 61 (2001) 1855–1861.
[46] Y. Jin, J.P. Li, L.Y. Tang, et al., Protein expression and significance of VEGF, EGFR and MMP-9 in non-small cell lung carcinomas, Asian Pacific J. Cancer Prev. 12 (2011) 1473–1476.
[47] J.L. Hsu, M.-C. Hung, The role of HER2, EGFR, and other receptor tyrosine kinases in breast cancer, Cancer Metastasis Rev. 35 (4) (2016) 575–588.
[48] A. Citri, Y. Yarden, EGF-ERBB signalling: towards the systems level, Nat. Rev. Mol. Cell Biol. 7 (2006) 505–516, https://doi.org/10.1038/NRM1962.
[49] Okabe T, Okamoto I, Tamura K, et al (2007) Differential constitutive activation of the epidermal growth factor receptor in non-small cell lung cancer cells bearing EGFR gene mutation and amplification. Cancer Res. 67:2046–2053. https://doi.org/10.1158/0008-5472.CAN-06-3339.
[50] Maegawa M, Takeuchi K, Funakoshi E, et al (2007) Growth Stimulation of Non–Small Cell Lung Cancer Cell Lines by Antibody against Epidermal Growth Factor Receptor Promoting Formation of ErbB2/ErbB3 Heterodimers. Mol Cancer Res 5:393–401. https://doi.org/10.1158/1541-7786.MCR-06-0303.
[51] Hirschhaeuser F, Sattler UGA, Mueller-Klieser W (2011) Lactate: A metabolic key player in cancer. Cancer Res 71:6921–6925. https://doi.org/10.1158/0008-5472.CAN-11-1457.
[52] G.A. Brooks, The Science and Translation of Lactate Shuttle Theory, Cell Metab. 27 (4) (2018) 757–785.
[53] A.P. Halestrap, The monocarboxylate transporter family-Structure and functional characterization, IUBMB Life 64 (1) (2012) 1–9.
[54] N. Draoui, O. Feron, Lactate shuttles at a glance: From physiological paradigms to anti-cancer treatments, DMM Dis Model Mech 4 (2011) 727–732, https://doi.org/10.1242/dmm.007724.
[55] Y. Contreras-Baeza, P.Y. Sandoval, R. Alarcón, A. Galaz, F. Cortés-Molina, K. Alegría, F. Baeza-Lehnert, R. Arce-Molina, A. Guequén, C.A. Flores, A. San Martín, L.F. Barros, Monocarboxylate transporter 4 (MCT4) is a high affinity transporter capable of exporting lactate in high-lactate microenvironments, J. Biol. Chem. 294 (52) (2019) 20135–20147.
[56] L. Tang, J. Liu, L. Zhu, Q. Chen, Z. Meng, L.i. Sun, J. Hu, Z. Ni, X. Wang, Curcumin Inhibits Growth of Human NCI-H292 Lung Squamous Cell Carcinoma Cells by Increasing FOXA2 Expression, Front. Pharmacol. 9 (2018), https://doi.org/10.3389/FPHAR.2018.00060.
[57] S.P. Banks-Schlegel, A F Gazdar CCH,, Intermediate filament and cross-linked envelope expression in human lung tumor cell lines - PubMed, Cancer Res. 45 (1985) 1187–1197.
[58] D.X. Nguyen, A.C. Chiang, X.-F. Zhang, J.Y. Kim, M.G. Kris, M. Ladanyi, W. L. Gerald, J. Massagué, WNT/TCF signaling through LEF1 and HOXB9 mediates lung adenocarcinoma metastasis, Cell 138 (1) (2009) 51–62.
[59] Y. Sasaki, T. Shinkai, K. Eguchi, T. Tamura, Y. Ohe, T. Ohmori, N. Saijo, Prediction of the antitumor activity of new platinum analogs based on their ex vivo pharmacodynamics as determined by bioassay, Cancer Chemother. Pharmacol. 27 (4) (1991) 263–270.
[60] K. Sellers, T.D. Allen, M. Bousamra, JinLian Tan, A. Méndez-Lucas, W. Lin, N. Bah, Y. Chernyavskaya, J.I. MacRae, R.M. Higashi, A.N. Lane, T.-M. Fan, M.O. Yuneva, Metabolic reprogramming and Notch activity distinguish between non-small cell lung cancer subtypes, Br. J. Cancer 121 (1) (2019) 51–64.
[61] Su H, Bodenstein C, Dumont RA, et al (2006) Monitoring tumor glucose utilization by positron emission tomography for the prediction of treatment response to epidermal growth factor receptor kinase inhibitors. Clin Cancer Res 12:5659–5667. https://doi.org/10.1158/1078-0432.CCR-06-0368.
[62] Rosa V De, Iommelli F, Monti M, et al (2015) Reversal of Warburg effect and reactivation of oxidative phosphorylation by differential inhibition of EGFR signaling pathways in non-small cell lung cancer. Clin Cancer Res. https://doi.org/10.1158/1078-0432.CCR-15-0375.
[63] Lim SO, Li CW, Xia W, et al (2016) EGFR signaling enhances aerobic glycolysis in triple negative breast cancer cells to promote tumor growth and immune escape. Cancer Res 76:1284. https://doi.org/10.1158/0008-5472.CAN-15-2478.
[64] Z. Weihua, R. Tsan, W.-C. Huang, Q. Wu, C.-H. Chiu, I.J. Fidler, M.-C. Hung, Survival of cancer cells is maintained by EGFR independent of its kinase activity, Cancer Cell 13 (5) (2008) 385–393.
[65] J. Garcia-Bermudez, L. Baudrier, K. La, et al., Aspartate is a limiting metabolite for cancer cell proliferation under hypoxia and in tumors, Nat. Cell Biol. 20 (2018) 775, https://doi.org/10.1038/S41556-018-0118-Z.
[66] J. Zhang, N.N. Pavlova, C.B. Thompson, Cancer cell metabolism: the essential role of the nonessential amino acid, glutamine, EMBO J. 36 (2017) 1302–1315, https://doi.org/10.15252/EMBJ.201696151.
[67] M. Momcilovic, S.T. Bailey, J.T. Lee, M.C. Fishbein, C. Magyar, D. Braas, T. Graeber, N.J. Jackson, J. Czernin, E. Emberley, M. Gross, J. Janes, A. Mackinnon, A. Pan, M. Rodriguez, M. Works, W. Zhang, F. Parlati, S. Demo, E. Garon, K. Krysan, T.C. Walser, S.M. Dubinett, S. Sadeghi, H.R. Christofk, D. B. Shackelford, Targeted Inhibition of EGFR and Glutaminase Induces Metabolic Crisis in EGFR Mutant Lung Cancer, Cell Rep. 18 (3) (2017) 601–610.
[68] M. Conrad, H. Sato, The oxidative stress-inducible cystine/glutamate antiporter, system x (c) (-): cystine supplier and beyond, Amino Acids 42 (2012) 231–246, https://doi.org/10.1007/S00726-011-0867-5.
[69] N. Wu, M. Yang, U. Gaur, H. Xu, Y. Yao, D. Li, Alpha-Ketoglutarate: Physiological Functions and Applications, Biomol Ther (Seoul) 24 (1) (2016) 1–8.
[70] A. Maus, G.J. Peters, Glutamate and α-ketoglutarate: key players in glioma metabolism, Amino Acids 49 (2017) 21–32, https://doi.org/10.1007/S00726-016-2342-9/FIGURES/4.
[71] R. Gorgoglione, V. Impedovo, C.L. Riley, D. Fratantonio, S. Tiziani, L. Palmieri, V. Dolce, G. Fiermonte, Vol 14, Page 14 (1) (2022) 245.
[72] N. Jyotsana, K.T. Ta, K.E. DelGiorno, The Role of Cystine/Glutamate Antiporter SLC7A11/xCT in the Pathophysiology of Cancer, Front. Oncol. 12 (2022) 1–13, https://doi.org/10.3389/FONC.2022.858462/BIBTEX.
[73] Bergman BC, Butterfield GE, Wolfel EE, et al (1999) Evaluation of exercise and training on muscle lipid metabolism. Am J Physiol 276:. https://doi.org/10.1152/AJPENDO.1999.276.1.E106.
[74] G.A. Brooks, Lactate shuttles in nature, Biochem. Soc. Trans. 30 (2002) 258–264, https://doi.org/10.1042/BST0300258.
[75] G.A. Brooks, Cell-cell and intracellular lactate shuttles, J. Physiol. 587 (2009) 5591–5600, https://doi.org/10.1113/jphysiol.2009.178350.
[76] I. San-Millán, C.G. Julian, C. Matarazzo, J. Martinez, G.A. Brooks, Is Lactate an Oncometabolite? Evidence Supporting a Role for Lactate in the Regulation of Transcriptional Activity of Cancer-Related Genes in MCF7 Breast Cancer Cells, Front. Oncol. 9 (2019), https://doi.org/10.3389/FONC.2019.01536.
[77] D.i. Zhang, Z. Tang, H.e. Huang, G. Zhou, C. Cui, Y. Weng, W. Liu, S. Kim, S. Lee, M. Perez-Neut, J. Ding, D. Czyz, R. Hu, Z. Ye, M. He, Y.G. Zheng, H.A. Shuman, L. Dai, B. Ren, R.G. Roeder, L. Becker, Y. Zhao, Metabolic regulation of gene expression by histone lactylation, Nature 574 (7779) (2019) 575–580.
[78] K. Leithner, A. Hrzenjak, M. Trötzmüller, T. Moustafa, H.C. Köfeler, C. Wohlkoenig, E. Stacher, J. Lindenmann, A.L. Harris, A. Olschewski, H. Olschewski, PCK2 activation mediates an adaptive response to glucose depletion in lung cancer, Oncogene 34 (8) (2015) 1044–1050.
[79] J. Zhao, J. Li, T.W.M. Fan, S.X. Hou, Glycolytic reprogramming through PCK2 regulates tumor initiation of prostate cancer cells, Oncotarget 8 (2017) 83602, https://doi.org/10.18632/ONCOTARGET.18787.
[80] J. Serpa, Cysteine as a Carbon Source, a Hot Spot in Cancer Cells Survival, Front. Oncol. 10 (2020), https://doi.org/10.3389/fonc.2020.00947.
[81] J.S. Biscardi, M.-C. Maa, D.A. Tice, M.E. Cox, T.-H. Leu, S.J. Parsons, c-Src-mediated phosphorylation of the epidermal growth factor receptor on Tyr845 and Tyr1101 is associated with modulation of receptor function, J. Biol. Chem. 274 (12) (1999) 8335–8343.
[82] L. Jin, J. Chun, C. Pan, G.N. Alesi, D. Li, K.R. Magliocca, Y. Kang, Z.G. Chen, D. M. Shin, F.R. Khuri, J. Fan, S. Kang, Phosphorylation-mediated activation of LDHA promotes cancer cell invasion and tumour metastasis, Oncogene 36 (27) (2017) 3797–3806.

[83] L.u. Gao, Q.-H. Xu, L.-N. Ma, J. Luo, K.P. Muyayalo, L.-L. Wang, D.-H. Huang, X.-J. Xiao, S.-B. Cheng, G. Mor, A.-H. Liao, Trophoblast-derived Lactic Acid Orchestrates Decidual Macrophage Differentiation via SRC/LDHA Signaling in Early Pregnancy, Int. J. Biol. Sci. 18 (2) (2022) 599–616.

[84] Q. Zheng, Y. Huang, H. Zhao, Y. Yang, S. Hong, X. Hou, Y. Zhao, Y. Ma, T. Zhou, Y. Zhang, W. Fang, L.i. Zhang, EGFR mutation genotypes affect efficacy and resistance mechanisms of osimertinib in T790M-positive NSCLC patients, Transl Lung Cancer Res 9 (3) (2020) 471–483.

[85] Y.-H. Huang, K.-H. Hsu, J.-S. Tseng, K.-C. Chen, C.-H. Hsu, K.-Y. Su, J.J.W. Chen, H.-W. Chen, S.-L. Yu, T.-Y. Yang, G.-C. Chang, The Association of Acquired T790M Mutation with Clinical Characteristics after Resistance to First-Line Epidermal Growth Factor Receptor Tyrosine Kinase Inhibitor in Lung Adenocarcinoma, Cancer Res. Treat. 50 (4) (2018) 1294–1303.

[86] B. Zou, V.H.F. Lee, L. Chen, L. Ma, D.D. Wang, H. Yan, Deciphering mechanisms of acquired T790M mutation after EGFR inhibitors for NSCLC by computational simulations, Sci. Rep. 7 (1) (2017), https://doi.org/10.1038/S41598-017-06632-Y.

[87] S. Kobayashi, T.J. Boggon, T. Dayaram, P.A. Jänne, O. Kocher, M. Meyerson, B. E. Johnson, M.J. Eck, D.G. Tenen, B. Halmos, EGFR mutation and resistance of non-small-cell lung cancer to gefitinib, N. Engl. J. Med. 352 (8) (2005) 786–792.

[88] A. Silva, B. Antunes, A. Batista, F. Pinto-Ribeiro, F. Baltazar, J. Afonso, In Vivo Anticancer Activity of AZD3965: A Systematic Review, Molecules 27 (1) (2022) 181.

[89] E.S. Reckzeh, H. Waldmann, Small-Molecule Inhibition of Glucose Transporters GLUT-1–4, Chembiochem 21 (1-2) (2020) 45–52.

[90] D. Benjamin, M.N. Hall, Combining metformin with lactate transport inhibitors as a treatment modality for cancer - recommendation proposal, Front. Oncol. 12 (2022) 5978, https://doi.org/10.3389/FONC.2022.1034397/BIBTEX.

[91] S. Suzuki, M. Okada, H. Takeda, K. Kuramoto, T. Sanomachi, K. Togashi, S. Seino, M. Yamamoto, T. Yoshioka, C. Kitanaka, Involvement of GLUT1-mediated glucose transport and metabolism in gefitinib resistance of non-small-cell lung cancer cells, Oncotarget 9 (66) (2018) 32667–32679.